Precision tests of the J/ψ from full lattice QCD: mass, leptonic width and radiative decay rate to η_c

G. C. Donald,[1] C. T. H. Davies,[1,*] R. J. Dowdall,[1] E. Follana,[2]
K. Hornbostel,[3] J. Koponen,[1] G. P. Lepage,[4] and C. McNeile[5]
(HPQCD collaboration)[,†]

[1]*SUPA, School of Physics and Astronomy, University of Glasgow, Glasgow, G12 8QQ, UK*
[2]*Departamento de Física Teórica, Universidad de Zaragoza, E-50009 Zaragoza, Spain*
[3]*Southern Methodist University, Dallas, Texas 75275, USA*
[4]*Laboratory of Elementary-Particle Physics, Cornell University, Ithaca, New York 14853, USA*
[5]*Bergische Universität Wuppertal, Gaussstr. 20, D-42119 Wuppertal, Germany*

(Dated: October 16, 2012)

We calculate the J/ψ mass, leptonic width and radiative decay rate to $\gamma\eta_c$ from lattice QCD including u, d and s quarks in the sea for the first time. We use the Highly Improved Staggered Quark formalism and nonperturbatively normalised vector currents for the leptonic and radiative decay rates. Our results are: $M_{J/\psi} - M_{\eta_c} = 116.5(3.2)$MeV; $\Gamma(J/\psi \to e^+e^-) = 5.48(16)$keV; $\Gamma(J/\psi \to \gamma\eta_c) = 2.49(19)$keV. The first two are in good agreement with experiment, with $\Gamma(J/\psi \to e^+e^-)$ providing a test of a decay matrix element in QCD, independent of CKM uncertainties, to 2%. At the same time results for the time moments of the correlation function can be compared to values from the charm contribution to $\sigma(e^+e^- \to \text{hadrons})$, giving a 1.5% test of QCD. Our results show that an improved experimental error would enable a similarly strong test from $\Gamma(J/\psi \to \gamma\eta_c)$.

I. INTRODUCTION

Precision tests of lattice QCD against experiment are critical to provide benchmarks against which to calibrate the reliability of predictions from lattice QCD [1]. Most tests to date have relied on the spectrum of gold-plated hadron masses - for example, the mass of the D_s meson can be calculated in lattice QCD with an error of 3 MeV (having fixed the masses of the c and s masses from other mesons) and the result agrees with experiment [2, 3]. Here we give another such test by determining the mass of the J/ψ to a precision of 3 MeV.

Tests of decay matrix elements are harder to do very accurately. We need precision tests of these because it is the predictions of decay matrix elements from lattice QCD that enable, for example, progress with the flavor physics programme [4] of over-determining the CKM matrix to find signs of new physics [5]. The leptonic decay rate of the π via a W boson provides one such test. The QCD input to this is the pion decay constant, which is determined to 1% in lattice QCD [6]. If we take V_{ud} from nuclear β decay [7], we have a 2% determination of the leptonic decay rate to be compared to experiment. The leptonic decay rates of other charged pseudoscalars can also be determined to a few percent from lattice QCD [4] but then the comparison with experiment is generally needed to determine the appropriate CKM element. Independent tests of matrix elements, without CKM uncertainties, come only from electromagnetic decays. Here we provide two such tests through two different decay rates of the J/ψ: annihilation to e^+e^- via a photon and radiative decay to the η_c. We give the first results from full lattice QCD including u, d and s quarks in the sea, although earlier calculations have been done in quenched QCD [8] and including u and d sea quarks [9, 10].

We are able to determine these matrix elements to a few percent because of our development of an accurate and fully relativistic approach to c quarks (as well as u, d and s) in lattice QCD called the Highly Improved Staggered Quark (HISQ) formalism [11]. In this formalism we are able to normalise the vector current which mediates the electromagnetic decay accurately and nonperturbatively and we show how to do that here.

The layout of the paper is as follows: section II describes the lattice calculation and then section III gives results for the J/ψ mass, leptonic width (along with time moments of the J/ψ correlator) and radiative decay rate in turn. We compare our results to experiment and to previous lattice QCD calculations in section IV. Section V gives our conclusions. The Appendices discuss the more technical issues of discretisation errors and our two different methods for current renormalisation.

II. LATTICE CALCULATION

We use 6 ensembles of lattice gluon configurations at 4 different, widely separated, values of the lattice spacing, provided by the MILC collaboration [12]. The configurations include the effect of u, d and s quarks in the sea with the improved staggered (asqtad) formalism. The u and d masses are taken to be the same with $m_{u/d}/m_s$ approximately 0.2 on most of the ensembles. Based on our experience of other gold-plated mesons [2] we expect sea quark mass effects to be small for the J/ψ because it

*c.davies@physics.gla.ac.uk
†URL: http://www.physics.gla.ac.uk/HPQCD

Set	r_1/a	$au_0m_l^{asq}$	$au_0m_s^{asq}$	L_s/a	L_t/a	δx_l	δx_s
1	2.647(3)	0.005	0.05	24	64	0.11	0.43
2	2.618(3)	0.01	0.05	20	64	0.25	0.43
3	2.658(3)	0.01	0.03	20	64	0.25	-0.14
4	3.699(3)	0.0062	0.031	28	96	0.20	0.19
5	5.296(7)	0.0036	0.018	48	144	0.16	-0.03
6	7.115(20)	0.0028	0.014	64	192	0.17	0.04

TABLE I: Ensembles (sets) of MILC configurations used for this analysis. The sea asqtad quark masses m_l^{asq} ($l = u/d$) and m_s^{asq} are given in the MILC convention where u_0 is the plaquette tadpole parameter. The lattice spacing values in units of r_1 after 'smoothing' are given in the second column [12]. Here sets 1, 2 and 3 are 'coarse'; set 4, 'fine'; set 5 'superfine' and set 6 'ultrafine'. The size of the lattices is given by $L_s^3 \times L_t$. The final two columns give the difference between the sea quark mass and its physical value in units of the s quark mass [2].

has no valence light quarks. We can test this by comparison of results on sets 1 and 2 where the sea value of $m_{u,d}$ changes by a factor of two and with set 3 where the sea value of m_s changes by 70%. Table I lists the parameters of the ensembles.

The lattice spacing is determined on an ensemble-by-ensemble basis using a parameter r_1 that comes from fits to the static quark potential calculated on the lattice [12]. This parameter has small statistical/fitting errors but its physical value is not accessible to experiment and so must be determined using other quantities, calculated on the lattice, that are. We have determined $r_1 = 0.3133(23)$ fm using four different quantities ranging from the (2S-1S) splitting in the Υ system to the decay constant of the η_s (fixing f_K and f_π from experiment) [13]. Using our value for r_1 and the MILC values for r_1/a given in Table I we can determine a in fm on each ensemble or, equivalently, a^{-1} in GeV needed to convert lattice quantities to physical units.

On these ensembles we calculate c quark propagators using the HISQ action and combine them into meson correlation functions. The quark propagators are made from a 'random wall' source - a color 3-vector of U(1) random numbers - on a given timeslice to reduce the statistical noise. An added reduction comes from the use of a random starting point for the equally spaced time-sources we use on the coarse and fine ensembles. We include only connected correlation functions here - disconnected contributions for the J/ψ are related to its hadronic width which is in keV and therefore negligible here.

The c quark mass is tuned from the η_c meson mass [2]. The appropriate 'experimental' mass for the η_c for our calculations is 2.986(3) GeV, differing from the experimental result of 2.981(1) GeV [7] because of missing electromagnetic, η_c annihilation and c-in-the-sea effects that we estimate perturbatively [14]. The HISQ lattice c quark masses for the ensembles we are using were determined in [2].

Meson masses and decay constants are determined from simple '2-point' meson correlation functions made from combining quark propagators with appropriate spin matrices at source and sink to project onto the correct J^{PC}. For staggered quarks, where the spin degree of freedom has disappeared, the spin projection matrices are replaced with space-time-dependent phases of ± 1. Because of fermion-doubling, there are in fact 16 'tastes' of every meson made by combining a point-splitting of the quark and antiquark source and sink along with the appropriate ± 1 phases. The most accurate meson correlation functions come from either local or 1-link separated sources and sinks and we will restrict ourselves to these here. Because the taste-splittings are discretisation effects we are free to use whichever taste is the most convenient for a given calculation.

For the pseudoscalar mesons the mass differences between the different tastes have a simple picture with the mass increasing as the amount of point-splitting in the source/sink operator increases. The lightest mass particle is the Goldstone meson whose correlator is simply the modulus squared of the propagator and whose squared mass vanishes linearly with the quark mass. This is the one that is used to tune the quark mass. The other taste pseudoscalar mesons have a mass for which the difference of mass-squared with the Goldstone meson is a constant with quark mass which vanishes as $\alpha_s^2 a^2$. These taste-splitting discretisation errors are particularly small with the HISQ action [11]. They also become smaller, in proportion to the meson mass, as the meson mass increases and so are very small for mesons made of c quarks [11]. The mass difference between the Goldstone meson and the next heaviest pseudoscalar meson is visible, however. Both masses can be determined very accurately in lattice QCD because they both correspond to local operators. The Goldstone meson corresponds to the local γ_5 operator and the local non-Goldstone to the local $\gamma_0\gamma_5$ operator. We will use both of these mesons in our calculation of the radiative decay rate of the J/ψ.

Vector meson taste-splittings are significantly smaller than for pseudoscalars and typically not visible for light mesons above the statistical errors. For the charmonium vectors we use the local γ_i operator to determine the leptonic decay rate and two different 1-link split operators for the radiative decay. We discuss mass differences from taste-splittings further in Appendix A.

III. RESULTS

A. $M_{J/\psi}$

The determination of the mass of the J/ψ is most accurately done through the determination of the charmonium hyperfine splitting, i.e. the mass difference with the pseudoscalar η_c meson. For the η_c we use the Goldstone meson, as discussed in section II, because this is the most accurately determined in lattice QCD and is the meson

we use to fix the c quark mass. We studied this meson in detail in [2]. For the J/ψ we use the local γ_i operator to create and destroy the vector meson. The J/ψ correlators are then obtained by combining quark propagators from the default random wall with antiquark propagators from a source using the same random wall but patterned with phases, for example $(-1)^x$ for the vector polarised in the x direction. $(-1)^x$ is also inserted at the sink where the propagators are tied together.

The J/ψ and η_c correlators at zero spatial momentum are fit simultaneously so that correlations between them are taken into account. The fit form for the average J/ψ correlator as a function of time separation between source and sink, t, is:

$$\overline{C}_{2pt}(t) = \sum_{i_n,i_o} a_{i_n}^2 \,\mathrm{fn}(M_{i_n},t) - \tilde{a}_{i_o}^2 \,\mathrm{fo}(\tilde{M}_{i_o},t) \qquad (1)$$

with

$$\begin{aligned} \mathrm{fn}(M,t) &= e^{-Mt} + e^{-M(L_t-t)} \\ \mathrm{fo}(M,t) &= (-1)^{t/a}\mathrm{fn}(M,t) \end{aligned} \qquad (2)$$

and L_t the time extent of the lattice. $i_n = 0$ is the ground state and larger i_n values denote radial or other excitations with the same J^{PC} quantum numbers. The M_{i_n} are the masses of the corresponding particles. There are 'oscillating' terms coming from opposite parity states, denoted i_o. The Goldstone η_c meson has the same fit form except that there are no oscillating contributions (when the η_c is at rest). Note that we do not use any 'smearing' functions for the propagators at either source or sink.

To fit we use a number of exponentials i_n, and where appropriate i_o, in the range 2–6, loosely constraining the higher order exponentials by the use of Bayesian priors [15]. As the number of exponentials increases, we see the χ^2 value fall below 1 and the results for the fitted values and errors for the parameters for the ground state $i = 0$ stabilise. This allows us to determine the ground state parameters a_0 and M_0 as accurately as possible whilst including the full systematic error from the presence of higher excitations in the correlation function. We take the fit parameters to be the logarithm of the ground state masses M_0 and $\tilde{M}_0$ and the logarithms of the differences in mass between successive radial excitations (which are then forced to be positive). The Bayesian prior value for M_0 for the η_c is obtained from a simple 'effective mass' in the correlator and the prior width on the value is taken as 0.3. The prior value on M_0 for the J/ψ is taken to be 100 ± 50 MeV above the η_c. The prior value for mass splittings to and between excitations is taken as 600(300) MeV. The amplitudes a_{i_n} and a_{i_o} are given prior widths of 1.0. We apply a cut on the range of eigenvalues from the correlation matrix that are used in the fit of 10^{-4}. We also cut out small t/a (and $(L_t - t)/a$) values below 6 from our fit to reduce the effect of higher excitations.

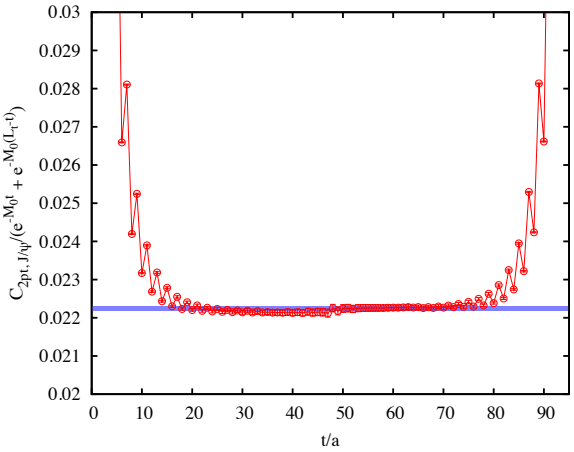

FIG. 1: Our average J/ψ correlator divided by the ground state exponential ($\mathrm{fn}(M_0,t)$ from eq. (2)) as a function of lattice time. Lines are drawn to join the points (which include statistical errors) for clarity. The fitted result for the ground state amplitude, a_0^2, is given by the blue band. The fit includes 6 normal exponentials and 6 oscillating ones, which are responsible for the oscillating behaviour clearly seen in the results.

Figure 1 shows the quality of our results with a plot of the J/ψ correlation function. It is divided by the ground-state exponential function so that it shows a plateau in the centre of value a_0^2. The results for the ground-state masses in lattice units of the J/ψ and η_c and the difference between them, $a\Delta M_{hyp}$, are given in Table II. The difference is typically more accurate than that obtained by simply subtracting the masses because of the correlation between the correlators.

The hyperfine splitting is converted to physical units using the values for a on each ensemble as discussed in section II. The results are shown in Figure 2. Figure 2 includes the error from the determination of the lattice spacing on each point. This dominates the error but is correlated between the points and that should be borne in mind in looking at the figure. It is important to realise that the naive lattice spacing error is magnified by a factor of approximately two in the hyperfine splitting because of the inverse relationship between hyperfine splitting and quark mass. For example, a shift by uncertainty δ upwards in the inverse lattice spacing causes a shift upwards in the meson mass by the same proportion. To determine the total effect of this on the hyperfine splitting we must include the effect of retuning the c quark mass to make the meson mass correct again. This means in this case retuning the quark mass down by fraction δ which shifts the hyperfine splitting upward by a further factor of δ to that coming simply from the lattice spacing change. Thus the change in the hyperfine splitting, rep-

Set	$N_{\rm cfg} \times N_t$	$m_c a$	ϵ	aM_{η_c}	$aM_{J/\psi}$	$a\Delta M_{hyp}$	$af_{J/\psi}/Z$	Z_{cc}
1	2099×8	0.622	-0.221	1.79118(4)	1.85934(8)	0.06817(6)	0.2810(2)	0.979(12)
2	2259×4	0.63	-0.226	1.80851(5)	1.87797(10)	0.06946(8)	0.2855(2)	0.979(12)
2	2259×8	0.66	-0.244	1.86667(4)	1.93430(9)	0.06763(7)	0.2925(2)	0.974(12)
3	323×8	0.617	-0.218	1.78212(12)	1.85081(23)	0.06869(17)	0.2804(5)	0.979(12)
4	566×4	0.413	-0.107	1.28052(7)	1.32901(12)	0.04849(10)	0.1829(2)	0.983(12)
5	200×2	0.273	-0.0487	0.89948(8)	0.93369(13)	0.03421(11)	0.1244(3)	0.986(12)
6	208×1	0.193	-0.0247	0.66649(6)	0.69217(11)	0.02568(10)	0.0925(3)	0.990(12)

TABLE II: Results in lattice units for the masses of η_c and J/ψ and their difference on each ensemble along with the raw (unrenormalised) decay constant and Z factor for the J/ψ. Columns 3 and 4 give the bare HISQ charm quark mass, tuned from the η_c and the corresponding coefficient ϵ used in the Naik discretization improvement term of the HISQ action [2]. All of the charm quark masses are very well tuned except for the lower result on set 2 ($m_c a = 0.66$), which was deliberately mistuned to assess the sensitivity of quantities to the tuning. Of the remaining masses the least well-tuned is on superfine set 5 where M_{η_c} is 0.5% too high. Column 2 gives the number of configurations used and the number of time sources for propagators on each configuration. Results are binned on time sources and binned over neighbouring configurations for sets 5 and 6. The J/ψ correlators are averaged over polarisations except on sets 2 and 3 where only one polarisation was calculated. The results for the η_c masses are also given in [2]. They differ slightly from these in some cases because of fitting simultaneously with J/ψ correlators. The Z factors are taken from moment 4 of the nonperturbative (on the lattice) current-current correlator method described in Appendix B 1.

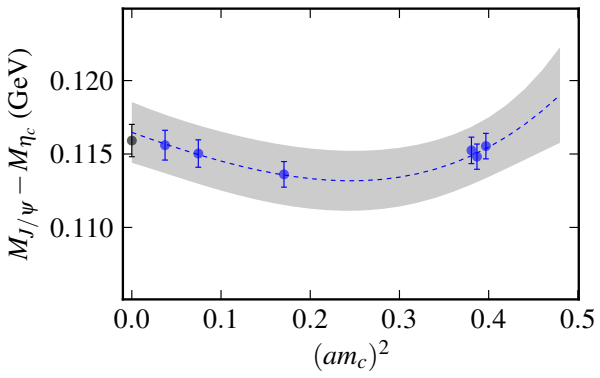

FIG. 2: Results for the charmonium hyperfine splitting plotted as a function of lattice spacing. For the x-axis we use $(m_c a)^2$ to allow the a-dependence of our fit function (eq. (3)) (blue dashed line with grey error band) to be displayed simply. The data points have been corrected for c quark mass mistuning and sea quark mass effects, but the corrections are smaller than the error bars. We do not include on the plot the deliberately mistuned c mass but it is included in the fit to constrain the c mass dependence. The errors shown include (and are dominated by) uncertainties from the determination of the lattice spacing a (from the physical value of the parameter r_1) that are correlated between the points. The experimental average is plotted as the black point at the origin, offset slightly from the y-axis for clarity.

resenting its uncertainty, is approximately 2δ [16][1]. Thus lattice spacing uncertainties are typically much more important in the determination of hyperfine splittings than statistical errors.

We fit the hyperfine splitting as a function of lattice spacing and sea quark masses to the form:

$$\begin{aligned} f(a,\delta x_l,\delta x_s) &= f_0 \times \\ &\sum_{ijkl} c_{ijkl}(am_c)^{2i}(\frac{\delta x_1}{10})^j(\frac{\delta x_2}{10})^k(\frac{\delta x_3}{10})^l \\ &+ (d_0 + d_1(am_c)^2)(M_{\eta_c,\rm latt} - M_{\eta_c,\rm expt}). \end{aligned} \quad (3)$$

Here f_0 is the physical result, the sum over $ijkl$ allows for discretisation errors and sea quark effects and the final term allows for mistuning of the c quark mass. We allow the discretisation errors, which are evident in our results, to have a scale set by the c quark mass. These appear only as even powers of a for staggered quarks. δx_l and δx_s are the mistuning of the sea quark masses:

$$\delta x_q = \frac{m_{q,\rm sea} - m_{q,\rm phys}}{m_{s,\rm phys}}. \quad (4)$$

δx_l and δx_s values are given for each ensemble in Table I and are taken from Appendix A of [2]. Eq. (3) includes a term for each sea quark (u/d appearing twice, and s), with the coefficients constrained to be the same so that the fit function is symmetric with respect to interchange of any two. The division by 10 is because the scale for dependence on light quark masses from chiral perturbation theory is $4\pi f_\pi \approx 10 m_s$. We see no significant sea quark mass dependence in the hyperfine splitting. A fairly strong dependence was seen in the twisted mass calculations [10]. However, at least some of that dependence could be attributed to the sea quark mass dependence of the lattice spacing, since that is determined only in the chiral limit. Here we determine the lattice spacing for each ensemble and hence separate lattice spacing dependence from physical sea quark mass effects. The sum over $ijkl$ in eq. (3) allows for the possibility of lattice spacing dependent sea quark mass effects.

[1] This point has frequently been overlooked in lattice QCD calculations.

We take a Bayesian prior [15] on f_0 of 0.1(1) and then fix c_{0000} to 1. The other c_{ijkl} are given priors of 0.0 ± 1.0 except for the c_{0jkl} which determine the a-independent sea quark mass dependence. These are taken to have priors 0.0 ± 0.33 because we expect sea quark mass effects to be typically a factor of 3 smaller than valence quark mass effects which would have chiral perturbation theory coefficients of $\mathcal{O}(1)$. We include 5 terms in the a-dependence and 3 in the δx dependence. Including additional terms makes no difference to the value for f_0 or its error. The priors for d_0 and d_1 are taken as 0.00(5), informed by the expectation that the hyperfine splitting should be inversely proportional to the mass, and by the effect of our mistuned c mass on set 2 which agrees roughly with that expectation.

The fit gives $f_0 = 116.5(2.1)$MeV, as the result for the hyperfine splitting in the absence of electromagnetism, c-in-the-sea and $\overline{c}c$ annihilation. The first two affect the η_c and J/ψ equally and so have no effect on the hyperfine splitting. The third affects the η_c more than the J/ψ, which has negligible width. A perturbative estimate of the shift of the η_c mass resulting from its annihilation to two gluons [11] related this to the total η_c width and obtained a shift downwards of the η_c mass of 2.4 MeV[2]. Using this, we have since applied a shift of 2.4(1.2) MeV for this effect to determine the η_c mass to which to tune our c quark mass, as in section II. For this purpose the impact of the shift is completely negligible, amounting to less than 0.1% of the η_c mass. For the hyperfine splitting, however, this shift could be a relatively large effect. Nonperturbative calculations of the contribution of 'disconnected diagrams' to the η_c mass have agreed on a small value of a few MeV for the shift from η_c annihilation but obtained the opposite sign [17]. The argument is that the perturbative result may be modified significantly by the gg intermediate state forming a resonance such as a glueball which is lighter in mass than the η_c, or a lighter hadron state. To allow for this possibility and be consistent with the nonperturbative calculations we do not apply a shift to the hyperfine splitting obtained from our fit above, but instead take an additional systematic error of 2.4 MeV, corresponding to our original shift, to allow for the effect.

Our final result for the hyperfine splitting is then:

$$\Delta M_{\rm hyp} = 116.5(2.1)(2.4)\,{\rm MeV} \tag{5}$$

where the errors are in turn from statistics/fitting and η_c annihilation. The uncertainty from η_c annihilation dominates the error. A complete error budget is given in Table III.

This is to be compared to the difference of the experimental averages of the two masses of 115.9(1.1) MeV [7]. Quite a spread of results make up the average. Recent values tend to be at the lower end of the hyperfine splitting range. For example, the 2011 Belle result for the η_c mass gives a hyperfine splitting of $111.5(^{+2.5}_{-1.6})$ MeV [18], and a recent result from BESIII gives 112.6(0.9) MeV [19].

[2] This would now amount to 2.9 MeV given that the average experimental width of the η_c has increased to 30 MeV [7].

	$M_{J/\psi} - M_{\eta_c}$	$f_{J/\psi}$	$V_{J/\psi\to\eta_c\gamma}(0)$
$(am_c)^2$ extrapolation	0.45	0.45	3.5
statistics	0.50	0.41	0.74
lattice spacing	1.6	0.42	0.0
sea quark extrapolation	0.29	0.26	1.3
M_{η_c} tuning	0.11	0.09	0.0
Z	-	1.23	0.14
M_{η_c} annihilation	2.1	0.0	0.0
electromagnetism	0.0	0.5	0.5
Total (%)	2.7	1.5	3.8

TABLE III: Complete error budget for hyperfine splitting, leptonic width and vector form factor as a percentage of the final answer.

B. $\Gamma(J/\psi \to e^+e^-)$ and $R_{e^+e^-}$

The amplitude, a_0, from the fit in equation (1) to our J/ψ correlators is directly related to the matrix element for the local vector operator to create or destroy the ground-state vector meson from the vacuum. The vector meson decay constant, f_v, for meson v is defined by:

$$\langle 0|\overline{\psi}\gamma^i\psi|v\rangle = f_v m_v \epsilon^i \tag{6}$$

where ϵ^i is the meson polarization. f_v for the J/ψ is then determined from our lattice QCD correlators, in terms of the ground-state parameters from our fit (eq. (1)) by:

$$\frac{f_v}{Z} = a_0\sqrt{\frac{2}{M_0}}, \tag{7}$$

where Z is the renormalisation constant required to match the local vector current in lattice QCD used here to that of continuum QCD at each value of the lattice spacing.

f_v is clearly a measure of the internal structure of a meson and in turn is related to the experimentally measurable leptonic branching fraction:

$$\Gamma(v_h \to e^+e^-) = \frac{4\pi}{3}\alpha^2_{QED}e_h^2\frac{f_v^2}{m_v} \tag{8}$$

where e_h is the electric charge of the heavy quark in units of e (2/3 for c). The experimental average, $\Gamma(J/\psi \to e^+e^-) = 5.55(14)$keV [7] gives $f_{J/\psi} = 407(5)$ MeV, remembering that the electromagnetic coupling constant runs with scale and using $1/\alpha_{QED}(m_c) = 134$ [20]. This can then provide a test of QCD at the 1% level. Electromagnetic corrections are small since the J/ψ must decay to an odd number of photons [21].

Our results for $f_{J/\psi}/Z$ are given in Table II. The final column of that table gives the values of Z determined from current-current correlators as described in Appendix B. This method uses continuum perturbation theory through $\mathcal{O}(\alpha_s^3)$ to normalise the lattice QCD correlators at small times. Z then results from a combination of non-perturbative lattice QCD calculations with continuum perturbation theory in a similar approach to that of the RI-MOM scheme[3] used to renormalise the currents for the same calculation using twisted mass quarks in [10]. The current-current correlator method has the advantage that we can use the same correlators from which we also extract, at large times, the nonperturbative information on the ground-state mass and decay constant. Indeed this allows some cancellation of discretisation errors apparent in the unrenormalized decay constant.

Multiplying $f_{J/\psi}/Z$ by Z and then by a^{-1} in GeV gives the physical results for the decay constant plotted in Figure 3. We fit these to the same function of lattice spacing and sea quark mass used for the hyperfine splitting, eq. (3). The only differences are that the prior on f_0 is taken as 0.5(5) in this case and the priors on the slope of the variation of $f_{J/\psi}$ with M_{η_c} are taken as: d_0, 0.065(5) and d_1, 0.00(25). These are informed by the variation we see for the deliberately mistuned c mass on set 2 and also by our extensive study of the behaviour of f_{η_c} with M_{η_c} in [2]. There we find a strong a-dependence in the slope of the decay constant with mass and so we allow for that here.

The physical result that we obtain in the continuum limit is:

$$f_{J/\psi} = 405(6)(2)\text{MeV}. \tag{9}$$

The first error is from the fit and is dominated by the error from the Z factor. The second error is an estimate of systematic effects from missing electromagnetism in our lattice QCD calculation [2]. The effect of missing c-in-the-sea is negligible in this case. A complete error budget is given in Table III.

The leptonic width is determined by the amplitude of the ground-state that dominates the correlator at large times. We can also determine the charm contribution to $R_{e^+e^-}$ through the time moments of the J/ψ correlator which depend on the behaviour at short times. The moments are defined by:

$$G_n^V = Z^2 C_n^V = Z^2 \sum_{\tilde{t}} \tilde{t}^n \overline{C}_{J/\psi}(\tilde{t}) \tag{10}$$

where $\tilde{t}$ is lattice time symmetrised around the centre of the lattice (see Appendix B). Results for $(G_n^V/Z^2)^{1/(n-2)}$ in lattice units on each of our ensembles are given in Table IV for $n = 4, 6, 8$ and 10. The power $1/(n-2)$ is

[3] This method is often called 'nonperturbative' in the lattice QCD literature.

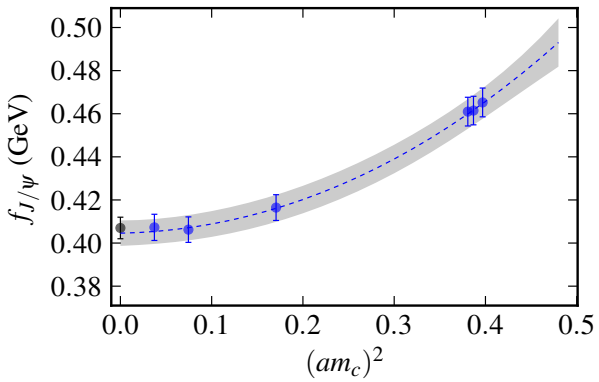

FIG. 3: Results for the charmonium vector decay constant plotted as a function of lattice spacing. For the x-axis we use $(m_c a)^2$ to allow the a-dependence of our fit function (eq. (3)) (blue dashed line with grey error band) to be displayed simply. The data points have been corrected for c quark mass mistuning and sea quark mass effects, but the corrections are smaller than the error bars. We do not include on the plot the deliberately mistuned c mass but it is included in the fit to constrain the c mass dependence. The errors shown include (and are dominated by) uncertainties from the determination of the current renormalization factor, Z, that are correlated between the points. The experimental average is plotted as the black point at the origin, offset slightly from the y-axis for clarity.

taken to reduce all the moments to the same dimension. We take the Z factor for the vector current to be the same one used for the leptonic width above, determined in Appendix B. Figure 4 then shows the physical results for the moments as a function of lattice spacing. The gray bands show our fits which use the same function of lattice spacing and sea quark masses as given in eq. (3). We reduce the prior width on the lattice spacing dependent terms by a factor of 4 because the moments are not as sensitive to short distances as the leptonic width or hyperfine splitting.

The physical results that we obtain for each moment in the continuum limit are given by:

$$\begin{aligned}
(G_4^V)^{1/2} &= 0.3152(41)(9)\,\text{GeV}^{-1} \\
(G_6^V)^{1/4} &= 0.6695(57)(13)\,\text{GeV}^{-1} \\
(G_8^V)^{1/6} &= 0.9967(65)(10)\,\text{GeV}^{-1} \\
(G_{10}^V)^{1/8} &= 1.3050(65)(6)\,\text{GeV}^{-1}.
\end{aligned} \tag{11}$$

The first error comes from the fit and the second allows for electromagnetism (e.g. photons in the final state) missing from our calculation but present in experiment. The error is estimated by substituting α_{QED} for α_s in the perturbative QCD analysis of the moments [22]. A complete error budget for our results is given in Table V.

The results agree well with the values extracted for the q^2 derivative moments, $\mathcal{M}_k$ $(n = 2k+2)$, of the charm quark vacuum polarization using experimental values for

Set	$m_c a$	$\left(\frac{G_4^V}{Z^2a^2}\right)^{1/2}$	$\left(\frac{G_6^V}{Z^2a^4}\right)^{1/4}$	$\left(\frac{G_8^V}{Z^2a^6}\right)^{1/6}$	$\left(\frac{G_{10}^V}{Z^2a^8}\right)^{1/8}$
1	0.622	0.5399(1)	1.2162(1)	1.7732(1)	2.2780(1)
2	0.63	0.5339(1)	1.2054(1)	1.7581(1)	2.2584(1)
2	0.66	0.5135(1)	1.1692(1)	1.7081(1)	2.1941(1)
3	0.617	0.5434(1)	1.2223(1)	1.7817(1)	2.2888(1)
4	0.413	0.7586(1)	1.6351(1)	2.3887(2)	3.0952(2)
5	0.273	1.0681(1)	2.2705(2)	3.3454(3)	4.3601(4)
6	0.193	1.4323(3)	3.0397(5)	4.4990(7)	5.8738(8)

TABLE IV: Results in lattice units for time moments of the J/ψ correlator as defined in eq. (10). We give results for n=4, 6, 8 and 10.

	$(G_4^V)^{1/2}$	$(G_6^V)^{1/4}$	$(G_8^V)^{1/6}$	$(G_{10}^V)^{1/8}$
$(am_c)^2$ extrapolation	0.18	0.18	0.16	0.16
statistics	0.05	0.04	0.03	0.03
lattice spacing	0.32	0.51	0.43	0.30
sea quark extrapolation	0.14	0.13	0.12	0.12
M_{η_c} tuning	0.15	0.18	0.17	0.16
Z	1.23	0.61	0.41	0.31
electromagnetism	0.3	0.2	0.1	0.05
Total (%)	1.3	0.9	0.7	0.5

TABLE V: Complete error budget for the time moments of the J/ψ correlator as a percentage of the final answer.

$R_{e^+e^-} = \sigma(e^+e^- \to \text{hadrons})/\sigma_{pt}$ [22, 23]. The values, extracted from experiment by [22] and appropriately normalised for the comparison to ours, are:

$$\begin{aligned}(M_1^{\rm exp}4!/(12\pi^2 e_c^2))^{1/2} &= 0.3142(22)\,{\rm GeV}^{-1}\\ (M_2^{\rm exp}6!/(12\pi^2 e_c^2))^{1/4} &= 0.6727(30)\,{\rm GeV}^{-1}\\ (M_3^{\rm exp}8!/(12\pi^2 e_c^2))^{1/6} &= 1.0008(34)\,{\rm GeV}^{-1}\\ (M_4^{\rm exp}10!/(12\pi^2 e_c^2))^{1/8} &= 1.3088(35)\,{\rm GeV}^{-1}. \quad (12)\end{aligned}$$

Our results from lattice QCD have approximately double the error of the experimental values but together these results provide a further test of QCD to better than 1.5%.

C. $\Gamma(J/\psi \to \gamma\eta_c)$

The radiative decay of the J/ψ meson to the η_c requires the emission of a photon from either the charm quark or antiquark and a spin-flip, so it is an M1 transition. Because it is sensitive to relativistic corrections this rate is hard to predict in nonrelativistic effective theories and potential models (see, for example, [24, 25]) Here we use a fully relativistic method in lattice QCD with a nonperturbatively determined current renormalisation and so none of these issues apply. In addition, of course, the lattice QCD result is free from model-dependence.

The quantity that parameterises the nonperturbative QCD information (akin to the decay constant of the previous section) is the vector form factor, $V(q^2)$, where q^2 is the square of the 4-momentum transfer from J/ψ to

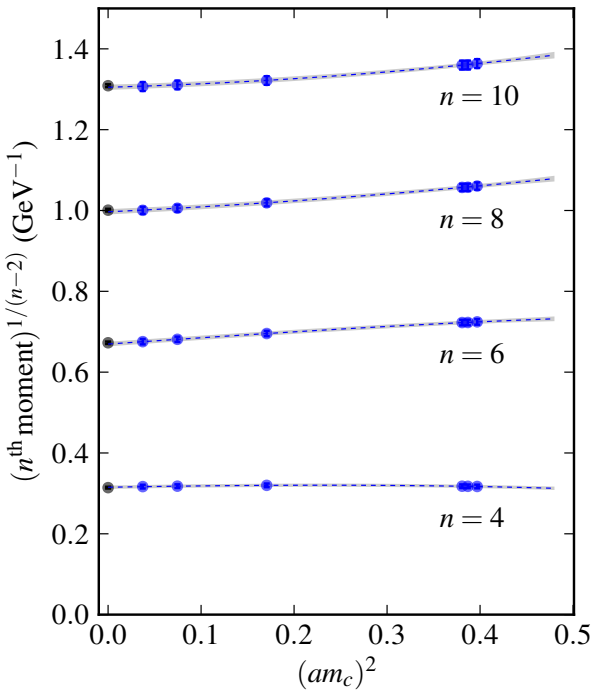

FIG. 4: Results for the 4th, 6th, 8th and 10th time moments of the charmonium vector correlator shown as blue points and plotted as a function of lattice spacing. The errors shown (the same size or smaller than the points) include (and are dominated by) uncertainties from the determination of the current renormalization factor, Z, that are correlated between the points. The data points have been corrected for c quark mass mistuning and sea quark mass effects, but the corrections are smaller than the error bars (the value for the deliberately mistuned c mass on set 2 is not shown). The blue dashed line with grey error band displays our continuum/chiral fit. Experimental results determined from $R_{e^+e^-}$ (eq. (12)) are plotted as the black points at the origin offset slightly from the y-axis for clarity.

η_c. The form factor is related to the matrix element of the vector current between the two mesons by:

$$\langle\eta_c(p')|\bar{c}\gamma^\mu c|J/\psi(p)\rangle = \frac{2V(q^2)}{(M_{J/\psi}+M_{\eta_c})}\varepsilon^{\mu\alpha\beta\gamma}p'_\alpha p_\beta \epsilon_{J/\psi,\gamma} \quad (13)$$

Note that the right-hand-side vanishes unless all the vectors are in different directions. Here we use a normalisation for $V(q^2)$ appropriate to a lattice QCD calculation in which the vector current is inserted in one c quark line only and the quark electric charge $(2e/3)$ is taken as a separate factor. The decay rate is then given by [8]:

$$\Gamma(J/\psi \to \eta_c\gamma) = \alpha_{QED}\frac{64|\vec{q}|^3}{27(M_{\eta_c}+M_{J/\psi})^2}|V(0)|^2, \quad (14)$$

where it is the form factor at $q^2 = 0$ that contributes because the real photon is massless. $|\vec{q}|$ is the corresponding momentum of the η_c in the J/ψ rest-frame.

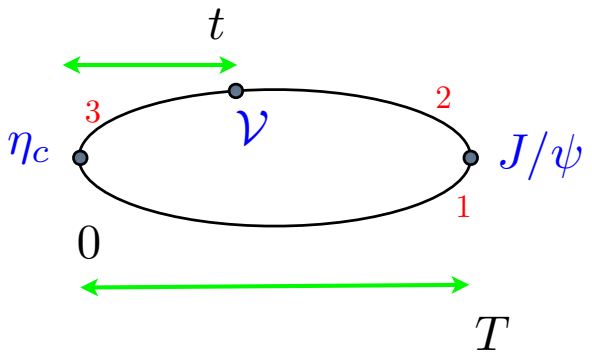

FIG. 5: A schematic diagram of the connected '3-point' function in lattice QCD for J/ψ to η_c radiative decay. The lines all represent c quark propagators in this case. The propagator labelled 1 is the spectator quark; 2 and 3 are the initial and final active quarks respectively. 0 and T label the position in time of the η_c and J/ψ operators. The vector current is inserted at time t which takes all values between 0 and T.

The most recent experimental result from CLEO-c [26] of 1.98(31)% for the branching fraction, combined with the total width of the J/ψ of 92.9(2.8) keV [7] gives

$$V(0)_{\rm expt} = 1.63(14), \tag{15}$$

where we have used $\alpha_{QED} = 1/137$ and $|\vec{q}| = (M_{J/\psi} - M_{\eta_c})(M_{J/\psi} + M_{\eta_c})/(2M_{J/\psi})$. The value of $|\vec{q}|$ from experiment is 0.1137(11) GeV where the error comes from the uncertainty in the η_c mass. $V(0)$ is then the quantity that can be calculated in lattice QCD and compared to experiment.

The radiative decay of the J/ψ to η_c meson needs the calculation of a '3-point' function in lattice QCD. The 3 points (in lattice time) correspond to: the position of the η_c operator, which we take as the origin; the position of the J/ψ operator which we denote T and the position of the insertion of a vector operator, $\mathcal{V} = \bar{c}\gamma_\mu c$, which couples to the photon at time t. t varies from 0 to T. Sums over spatial points are implied at each time. The 'connected' correlator that we calculate is illustrated in Figure 5. Disconnected correlators are expected to be negligible here based on perturbative and phenomenological arguments [8] and we do not include them.

The 3-point function is calculated in lattice QCD by combining 3 quark propagators together with appropriate spin projection matrices. As discussed in section II for staggered quarks these γ matrices become ± 1 phases. Tastes must be combined in a staggered quark correlator so that the overall correlation function is 'tasteless'. What this means for a 3-point function is that only certain taste combinations of J/ψ, η_c and $\mathcal{V}$ operators are allowed. To optimise statistical errors we need to keep to a minimum the amount of point-splitting in the operators. It is also convenient, for renormalisation purposes, to have a vector current, $\mathcal{V}$, which corresponds to a local operator (and this is also what we used for the decay constant in section III B).

We therefore choose the η_c operator to be the local γ_5 operator (so that the η_c is the Goldstone pseudoscalar with spin-taste $\gamma_5 \otimes \gamma_5$) and the J/ψ operator to be a one-link separated $\gamma_0\gamma_i$ operator in which the polarisation of the J/ψ and the one-link separation are both in an orthogonal spatial direction to the polarisation of the vector current, $\mathcal{V} = \bar{c}\gamma_k c$ (this J/ψ has spin-taste structure $\gamma_0\gamma_i \otimes \gamma_0\gamma_i\gamma_j$).

To implement this configuration is simple. The spectator quark propagator (number 1 in Figure 5) is generated from the default random wall at time 0. Active propagator 2 is then generated from a source which is made from a symmetric point-splitting of propagator 1 at time T patterned by a phase. For a J/ψ with polarisation x we take a point-splitting in the y direction and phase $(-1)^{x+z}$. Active propagator 3 is made from the same default random wall as 1. Finally 2 and 3 are combined together at t by summing over space with a patterning of $(-1)^z$ to implement a local vector current in the z direction.

To achieve the configuration corresponding to $q^2 = 0$ we keep the J/ψ at rest in the frame of the lattice and give the η_c an appropriate spatial momentum. The η_c momentum is implemented by calculating propagator 3 with a 'twisted boundary condition' [27, 28]. If propagator 3 is calculated with boundary condition:

$$\chi(x + \hat{e}_j L) = e^{2\pi i\theta_j}\chi(x), \tag{16}$$

then the momentum of the η_c meson made by combining propagators 1 and 3 with our random wall sources and summing over spatial sites at the sink is:

$$p_j = \frac{2\pi}{L_s}\theta_j. \tag{17}$$

The boundary condition in eq. (16) is actually implemented by multiplying the gluon links in the j direction by phase $\exp(2\pi i\theta_j/L_s)$. We take j to be the y direction here so that the momentum is in an orthogonal direction to the polarisation of both the J/ψ and $\mathcal{V}$.

The 3-point function is then given by:

$$C_{3pt}(0,t,T) = \sum_{s_T,s_t} \frac{1}{4}(-1)^{x_T+z_T}(-1)^{z_t} \times \tag{18}$$
$$\mathrm{Tr}\left\{g(t,T)[g(T+1_y,0) + g(T-1_y,0)]g^\dagger_\theta(t,0)\right\}$$

where g represent staggered c quark propagators, with g_θ computed with a phase on the gluon field, the trace is over color and sums are done over spatial sites s_t and s_T at t and T. The 1/4 is the taste factor for the normalisation of a staggered quark loop. The corresponding 2-point function for the η_c meson is

$$C_{\eta_c,2pt}(0,t) = \sum_{s_t} \frac{1}{4} \times \mathrm{Tr}\left[g(t,0)g^\dagger_\theta(t,0)\right]. \tag{19}$$

Set	$N_{\rm cfg} \times N_t$	T values	$m_c a$	$aM_{J/\psi}$ $\gamma_0\gamma_i \otimes \gamma_0\gamma_i\gamma_j$	aM_{η_c} $\gamma_5 \otimes \gamma_5$	$2\pi\theta$	$aE^{\theta}_{\eta_c}$	V^{nn}_{00}	$V(0)/Z$	Z_{ff}	a^2q^2
1	2088×4	15,18,21	0.622	1.86084(10)	1.79116(4)	1.6410	1.79243(4)	0.0362(2)	1.900(11)	0.9896(11)	$1(4) \times 10^{-5}$
2	2259×4	15,18,21	0.63	1.87972(12)	1.80842(7)	1.4007	1.81023(5)	0.0368(2)	1.897(12)	0.9894(8)	$-7(1) \times 10^{-5}$
		15,18,21	0.63	1.87962(14)	1.80839(8)	1.3880	1.81019(4)	0.0362(4)	1.883(20)	0.9894(8)	$1(5) \times 10^{-5}$
4	1911×4	20,23,26,29	0.413	1.32905(9)	1.28046(3)	1.3327	1.28133(3)	0.0348(2)	1.876(8)	1.0049(10)	$6(4) \times 10^{-5}$
				$\gamma_i \otimes \gamma_i\gamma_j$	$\gamma_0\gamma_5 \otimes \gamma_0\gamma_5$						
1	2088×4	15,18,21	0.622	1.86035(15)	1.79621(4)	1.5120	1.79725(4)	0.0338(6)	1.925(35)	0.9896(11)	$3(5) \times 10^{-5}$
2	2259×4	15,18,21	0.63	1.87887(13)	1.81369(6)	1.2814	1.81480(5)	0.0334(8)	1.896(45)	0.9894(8)	$0(4) \times 10^{-5}$
		15,18,21	0.66	1.93604(15)	1.87254(6)	1.2490	1.87355(6)	0.0322(8)	1.934(42)	0.9863(17)	$1(5) \times 10^{-5}$
4	1911×4	19,20,23,26	0.413	1.32904(11)	1.28160(4)	1.3116	1.28243(4)	0.0342(4)	1.872(21)	1.0049(10)	$-2(1) \times 10^{-5}$

TABLE VI: Results from simultaneous fits for 3-point and 2-point correlators for $J/\psi \to \gamma\eta_c$ decay. The upper table gives results from our preferred jpsigamma0 method; the lower table from etacgamma0. See the text for a definition of the two methods. Column 2 gives the number of configurations and time sources for 0 on each configuration. Column 3 gives the different values of the end-point of the 3-point function, T, included in the fit. The lattice c quark mass and ϵ parameter are the same as those used in section III A (the lower table includes the deliberately mistuned mass on set 2 for comparison). $aM_{J/\psi}$ and aM_{η_c} are the zero-momentum meson masses for the tastes of J/ψ and η_c mesons used here. $2\pi\theta$ indicates the value of the phase at the boundary used to achieve the kinematics of $q^2 = 0$ in the $J/\psi \to \eta_c$ decay. The a^2q^2 values actually obtained with those kinematics are given in the final column (rows 2 and 3 of the upper table compare two different values of a^2q^2 close to zero). aE_{η_c} gives the energy of the η_c at the value of the spatial momentum corresponding to θ. V^{00}_{nn} from the 3-point fit of eq (25) is given in column 9 and this is converted to a value of $V(0)/Z$ in column 10 using eq. (27). Column 11 gives the values of the renormalisation parameter, Z, obtained from the vector form factor method of Appendix B 2.

The 2-point function for the J/ψ is given by

$$C_{J/\psi,2pt}(0,t) = \sum_{s_t} \frac{1}{4}(-1)^{y_0+t_0}(-1)^{y_t+t_t} \times \qquad (20)$$
$$\mathrm{Tr}\left[g(t,0)(g^\dagger(t+1_y,1_y) + g^\dagger(t-1_y,1_y) + \{1 \leftrightarrow -1\})\right].$$

As an alternative configuration we can take the η_c operator to be the local $\gamma_0\gamma_5$ operator (so that the η_c is the local non-Goldstone meson with spin-taste structure $\gamma_0\gamma_5 \otimes \gamma_0\gamma_5$) and the J/ψ operator to be a one-link separated γ_i operator in which the polarisation of the J/ψ and the one-link separation are both in an orthogonal spatial direction to the polarisation of the vector current, $\mathcal{V}$ (this has spin-taste structure $\gamma_i \otimes \gamma_i\gamma_j$). The 3-point function is then given by:

$$C_{3pt}(0,t,T) = \sum_{s_T,s_t} \frac{1}{4}(-1)^{x_0+y_0+z_0}(-1)^{y_T}(-1)^{z_t} \times$$
$$\mathrm{Tr}\left[g(t,T)(g(T+1_y,0) + g(T-1_y,0))g^\dagger_\theta(t,0)\right] \qquad (21)$$

and the corresponding 2-point functions are:

$$C_{\eta_c,2pt}(0,t) = \sum_{s_t} \frac{1}{4}(-1)^{x_0+y_0+z_0}(-1)^{x_t+y_t+z_t} \times$$
$$\mathrm{Tr}\left[g(t,0)g^\dagger_\theta(t,0)\right]. \qquad (22)$$

and

$$C_{J/\psi,2pt}(0,t) = \sum_{s_t} \frac{1}{4}(-1)^{x_0+z_0+t_0}(-1)^{x_t+z_t+t_t} \times \qquad (23)$$
$$\mathrm{Tr}\left[g(t,0)(g^\dagger(t+1_y,1_y) + g^\dagger(t-1_y,1_y) + \{1 \leftrightarrow -1\})\right].$$

We call this configuration the 'etacgamma0' configuration and the original configuration of eq. (19) the 'jpsigamma0' configuration. In fact, as we shall see, the jpsigamma0 configuration is to be preferred on the basis of statistical errors but the results agree between the two.

The 3-point function in both cases is calculated along with the 2-point functions for the η_c and J/ψ mesons that appear in it. We use multiple time-sources for point 0 on each configuration and also multiple values for T. Figure 6 shows results for the 3-point function on fine set 4, normalising it to the product of the relevant 2-point functions. The two plots compare results for the jpsigamma0 method and the etacgamma0 method. The two differ in the amount of oscillation that is seen at the two ends of the plot. Not surprisingly the jpsigamma0 method shows more oscillation on the J/ψ end (t near T) since the η_c in this case would not oscillate at rest. The etacgamma0 method has relatively large oscillations for the η_c side but smaller oscillations on the J/ψ side. In both cases statistical errors are very small enabling us to fit both normal and oscillating terms. The figure also shows how having multiple T values improves our determination of the ground-state transition amplitude.

We fit the 3-point function and 2-point functions simultaneously to a multi-exponential that determines the ground-state amplitudes accurately because it includes excited state contributions. The fit form for the 2-point functions was already given in eq. (1). Here both the J/ψ and η_c correlators have oscillating contributions and, in the η_c case, the exponent gives the energy of the meson at momentum p_j (eq. (17)) rather than the mass. The

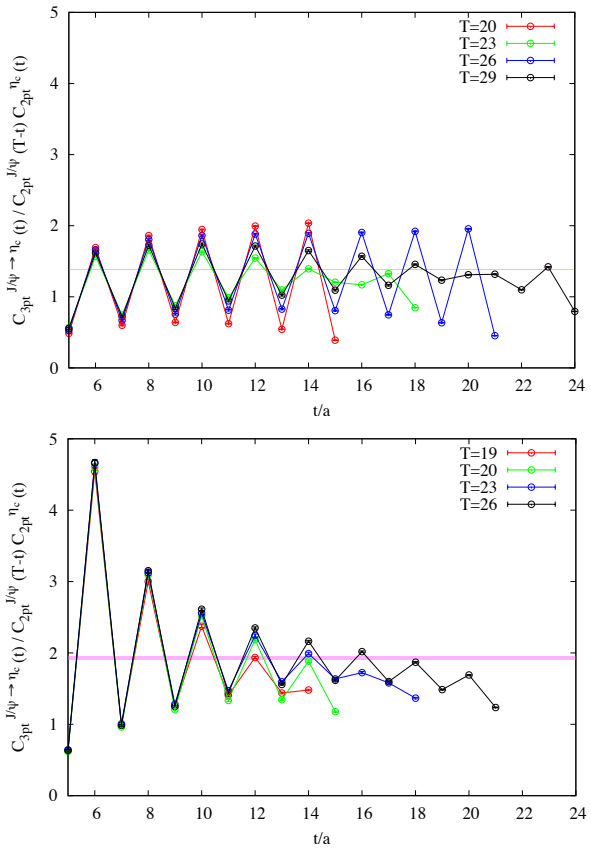

FIG. 6: A plot of the ratio $C_{3pt}(t,T)/(C_{2pt,\eta_c}(t)C_{2pt,J/\psi}(T-t))$ for the three values of T on the fine ensemble, set 4 and for our two different methods. Lines join the points (which have statistical errors on them) for clarity. We only include points in the central region of t i.e. $t \geq 5$ or $t \leq T-5$. The pink shaded band shows the ratio of fit parameters $V_{00}^{nn}/a_0 b_0$ which is the ground-state contribution to this ratio. These come from a fit that included 6 normal exponentials and 5 oscillating ones (which produce the oscillations evident in the figure). The top plot shows the results for the case where γ_0 is included in the J/ψ operator (jpsigamma0 method) and the lower plot shows the results for the case where γ_0 is included in the η_c operator (etacgamma0 method).

fit form for the 3-point function is then:

$$
\begin{aligned}
&C_{3pt}(t,T) = \qquad (24)\\
&\sum_{i_n,j_n} a_{i_n} \mathrm{fn}(E_{a,i_n},t) V^{nn}_{i_n,j_n} b_{j_n} \mathrm{fn}(E_{b,j_n},T-t)\\
&- \sum_{i_n,j_o} a_{i_n} \mathrm{fn}(E_{a,i_n},t) V^{no}_{i_n,j_o} \tilde{b}_{j_o} \mathrm{fo}(\tilde{E}_{b,j_o},T-t)\\
&- \sum_{i_o,j_n} \tilde{a}_{i_o} \mathrm{fo}(\tilde{E}_{a,i_o},t) V^{on}_{i_o,j_n} b_{j_n} \mathrm{fn}(E_{b,j_n},T-t)\\
&+ \sum_{i_o,j_o} \tilde{a}_{i_o} \mathrm{fo}(\tilde{E}_{a,i_o},t) V^{oo}_{i_o,j_o} \tilde{b}_{j_o} \mathrm{fo}(\tilde{E}_{b,j_o},T-t)
\end{aligned}
$$

and, again:

$$
\begin{aligned}
\mathrm{fn}(E,t) &= e^{-Et} + e^{-E(L_t-t)}\\
\mathrm{fo}(E,t) &= (-1)^{t/a}\mathrm{fn}(E,t) \qquad (25)
\end{aligned}
$$

with L_t again the time extent of the lattice. Here n denotes the normal contributions and o the contributions from oscillating states. The ground-state energies/masses that we need are $E_{\eta_c,0}$ and $E_{J/\psi,0} = M_{J/\psi}$ and the matrix element between them that is proportional to $V^{nn}_{0,0}$. By matching to a continuum correlator with a relativistic normalisation of states and allowing for a renormalisation of the lattice vector current we see that:

$$\langle \eta_c | V | J/\psi \rangle = 2Z\sqrt{M_{J/\psi} E_{\eta_c}} V^{nn}_{0,0}. \qquad (26)$$

The vector form factor that we need, $V(0)$, is then, from eq. (13), given by:

$$\frac{V(0)}{Z} = \frac{M_{J/\psi} + M_{\eta_c}}{2M_{J/\psi} p_j} 2\sqrt{M_{J/\psi} E_{\eta_c}} V^{nn}_{0,0}, \qquad (27)$$

with p_j from eq. (17). The determination of Z will be discussed below.

To perform the joint fit to the 3pt correlators using eq. (25) and the 2pt correlators using eq.(1) we use the same approach as outlined in section III A. For both the η_c and J/ψ, the prior for the ground-state mass comes from the effective mass of the correlator. We use priors of 600 MeV with a width of 300 MeV for the difference in mass between the ground state and the lowest oscillating mass and between all radial excitations, both normal and oscillating. The 2-point amplitudes, a_i and b_i, have prior widths of 0.5 and the 3-point amplitudes, V_{ij}, have widths of 0.25. We omit t values below a certain t_{min} to reduce the effect of excited states. $t_{\mathrm{min}} = 4(5)$ for the coarse(fine) lattices for the etacgamm0 method and 6 for the jpsigamm0 method.

Table VI gives our results from fits that include 6 normal exponentials and 5 oscillating. We work on ensembles 1, 2 and 4 of Table I but using more configurations than in section III A to reduce statistical errors. Table VI gives the number of configurations and time sources as well as the values of T used in the 3-point functions. It is important to use both even and odd values of T to separate clearly the normal and oscillating contributions. Having determined the mass of the local non-Goldstone η_c and 1-link vector from separate 2-point function fits we then determine the value of θ needed to achieve $q^2 = 0$. The final fits are done as a simultaneous fit to the 3-point function and 2-point functions for zero momentum and finite momentum η_c and zero momentum J/ψ.

The key parameters to be determined from the fit, as discussed above, are the ground-state masses of the η_c and J/ψ, the ground state energy at non-zero momentum of the η_c and the ground-state to ground-state amplitude of the 3-point function. Our fit returns excited

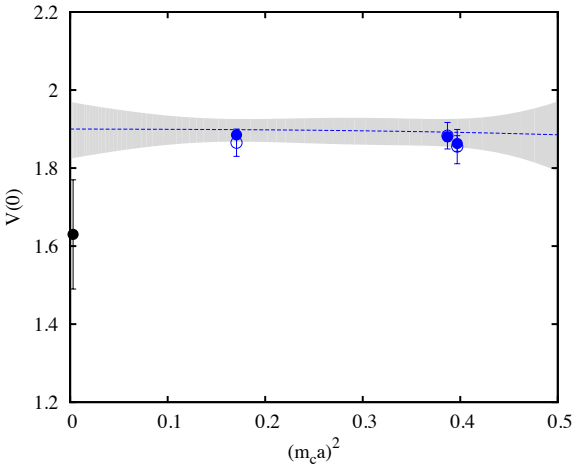

FIG. 7: Results for the vector form factor at $q^2 = 0$ for $J/\psi \to \eta_c$ decay plotted as a function of lattice spacing. The filled blue circles are from our preferred jpsigamma0 method; the open blue circles are from the etacgamma0 method. For the x-axis we use $(m_c a)^2$ to allow the a-dependence of our fit function to be displayed simply (blue dashed line and grey band). The fit is to results from the jpsigamma0 method. The errors shown include statistical errors and errors from the Z factor. The experimental result extracted from the branching fraction for $J/\psi \to \gamma\eta_c$ is plotted as the black point offset slightly from the origin for clarity.

state to ground-state and oscillating to ground state amplitudes also. Most of these do not have a significant signal. Indeed the excited state to ground state amplitudes are very small, as expected since they correspond to a hindered M1 transition. A non-zero result is seen for the transition between the oscillating partner of the η_c (in the etacgamma0 method) and the J/ψ. This corresponds to the E1 χ_{c0} to J/ψ decay, but not at the correct kinematics for that decay. Likewise a signal is seen for E1 $h_c \to \eta_c$ decay in jpsigamma0 method. We will discuss these transitions further elsewhere.

From eq. (27) we can determine $V(0)$ given a value for V_{00}^{nn} and a renormalisation factor, Z. For Z we use the fully nonperturbative vector form factor method described in Appendix B 2 which normalises the local charm-charm vector current that we are using here by demanding that its form factor is 1 between identical mesons at $q^2 = 0$. This requires a non-staggered spectator quark and we use NRQCD for this. The determination of Z_{ff} then needs the calculation of the form factor of the temporal component of the vector current between two B_c-like mesons (the mesons do not have to be real B_c mesons) at rest. Z_{ff} can be determined with a statistical uncertainty of 0.1% this way. Details are given in Appendix B 2.

The values for Z are given in Table IX of Appendix B 2 and the values we use here are reproduced in Table VI along with our results for V_{00}^{nn}, $V(0)/Z$ and the η_c and J/ψ masses and energies. The table is divided into two with the upper results from the jpsigamma0 method and the lower results from the etacgamma0 method. The two methods give results for $V(0)/Z$ in good agreement, but the jpsigamma0 results are statistically more accurate. This is then our preferred method and the one that we will use for our final result. The agreement between the two methods to within the 2% statistical errors is a strong test of the control of discretisation errors in the HISQ formalism.

Table IX also gives results that allow us to test to what extent $V(0)$ depends on m_c and the precise tuning of q^2 to zero. On set 2 we have deliberately mistuned the c quark mass by 5% and see that it makes no significant difference to $V(0)$ within our 2% statistical errors. q^2 is tuned to zero typically within our statistical errors of $(10\text{MeV})^2$. On set 2 comparison between two different values of q^2 shows no effect within our 1% statistical errors. We use the value closest to $q^2 = 0$ in our fits below. These are both good tests of the robustness of our results to the tuning of parameters.

Figure 7 shows our results for $V(0)$ plotted as a function of the lattice spacing. To determine the physical value we use a fit similar to that for the hyperfine splitting and leptonic decay constant given in eq. 3. We simplify the fit slightly in dropping the tuning for the physical c mass since our results in Table VI show negligible dependence on the c quark mass. We take the prior on the physical value to be 2.0(0.5) and allow for terms in $(m_c a)^{2i}$ up to $i = 5$. We take the prior on the leading $(m_c a)^2$ term to be 0.0(3) since tree-level a^2 errors are removed in the HISQ action. We take linear and quadratic terms in $2\delta x_l + \delta x_s$ and allow a^2 dependence multiplying the linear term.

The physical value for $V(0)$ from the fit is 1.90(7) from the jpsigamma0 method. The etacgamma0 method gives a result in good agreement with a very similar error. The error is dominated by that from the extrapolation in the lattice spacing. In fact there is no visible lattice spacing dependence in our results and it could be argued that, in a transition from J/ψ to η_c that probes relatively low momenta, the relevant scale for discretisation errors is well below m_c. However, to be conservative, we allow discretisation errors to depend on $(m_c a)^2$ and allow for multiple powers to appear.

We have also tested extrapolations of $V(0)$ to the physical point using alternative definitions of the renormalisation of the current. We get the same answer using Z_{ff} values taken from $B_c \to B_c$ form factors with a heavier b quark mass, as given in Appendix B 2. We also get a result in good agreement if we use values for Z from Z_{cc} given in Appendix B 1.

Our physical result for $V(0)$ is for a world that does not include electromagnetism, c-in-the-sea or allow for η_c annihilation. The effect of missing electromagnetism is similar to that for the decay constant and so we allow the same additional systematic error of 0.5%. We expect c-in the sea effects to be negligible, as for the decay constant. η_c annihilation affects the mass difference between

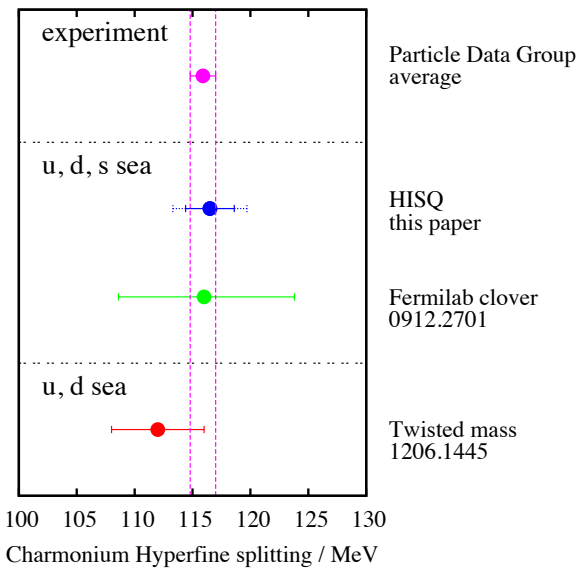

FIG. 8: A comparison of results for the charmonium hyperfine splitting from lattice QCD with experiment. We show only results that include sea quarks and make use of multiple lattice spacings to derive a continuum value. The experimental average [7] is given at the top, followed by the result for HISQ quarks from this paper. The Fermilab clover [29] and twisted mass [10] results follow. Neither of these lower two results include an error for missing η_c annihilation effects. This error is the dominant error for our calculation. Here we show our error bar excluding this effect as a solid line and the total error including this effect as a dotted line.

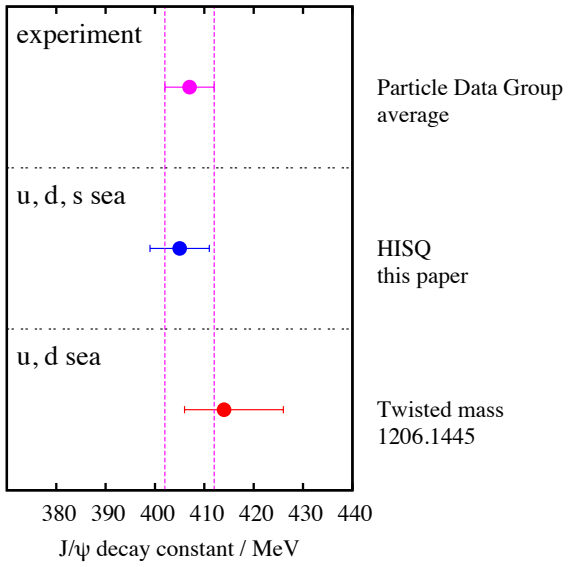

FIG. 9: A comparison of results for the decay constant of the J/ψ from lattice QCD with experiment. We include only results that include sea quarks and make use of multiple lattice spacings to derive a continuum value. The experimental average [7] is given at the top, followed by the result for HISQ quarks from this paper. The twisted mass [10] results follow.

the J/ψ and η_c (as discussed in section III A) and therefore affects the momentum of the η_c that corresponds to $q^2 = 0$ for this decay. Equivalently it means that the real $q^2 = 0$ point corresponds to a non-zero q^2 in our calculation. Since we allow an uncertainty in the η_c mass of 2.4 MeV (Table III) this corresponds to an uncertainty around $q^2 = 0$ of $6 \times 10^{-6}\text{GeV}^2$, keeping the spatial momentum fixed. From Table VI we see that this would produce a negligible change in $V(0)$, not visible beneath our statistical errors. In addition we can use information from [8] which used results at different q^2 values to extrapolate to $q^2 = 0$ albeit in the quenched approximation. The q^2 dependence gave a change in $V(q^2)$ from $V(0)$ of 20% when q^2 was 1GeV^2. From this it is clear that effects from a slight mistuning because of η_c annihilation effects should be completely negligible. We take as our final result then:

$$V(0) = 1.90(7)(1). \tag{28}$$

The complete error budget is given in Table III.

IV. DISCUSSION

Figure 8 compares our result for the charmonium hyperfine splitting to experiment and to that from other lattice QCD calculations. We only show results that have been obtained including sea quark effects and making use of multiple lattice spacing values to derive a physical continuum result. Values are also given for different forms of the clover action in [30–33] but either at only one value of the lattice spacing or without giving a value from continuum extrapolation. Some of these latter calculations obtain values well below experiment because of the large discretisation errors, particularly for the hyperfine interaction, in the clover formalism.

Our result agrees well with experiment and is more accurate than earlier values, especially since earlier values do not generally include any error for missing η_c annihilation effects.

Figure 9 similarly compares our result for $f_{J/\psi}$ to that from twisted mass quarks including only u and d quarks in the sea [10] and to experiment (from eq. (8)). Both lattice results agree well with experiment at the 2% level of accuracy achieved. Our value for $f_{J/\psi}$ gives a value for $\Gamma(J/\psi \to e^+e^-)$ of 5.48(16) keV using eq. (8).

Figure 10 shows the same comparison for the vector form factor at $q^2 = 0$, $V(0)$, for $J/\psi \to \eta_c\gamma$ decay. Our result here using HISQ quarks and including u, d and s quarks in the sea agrees well, at the 4% level of accuracy achieved, with the result using twisted mass quarks and including only u and d sea quarks.

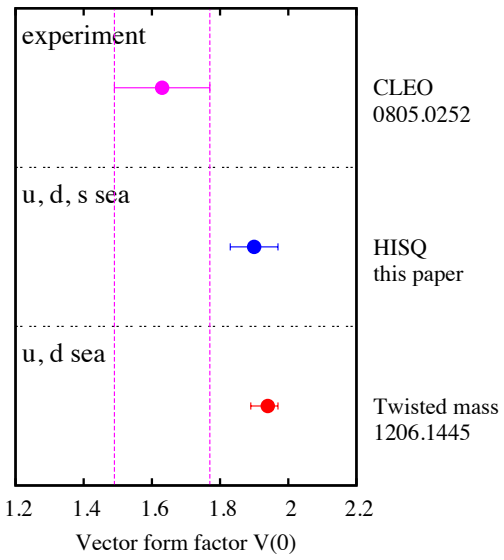

FIG. 10: A comparison of results for the vector form factor, $V(0)$ for $J/\psi \to \eta_c\gamma$ from lattice QCD with experiment. We include only results that include sea quarks and make use of multiple lattice spacings to derive a continuum value. The experimental result [26] is given at the top, followed by the result for HISQ quarks from this paper. The twisted mass [10] results follow.

The value of $V(0)$ extracted from the experimental branching fraction [26] is 1.7σ lower than the lattice numbers where σ is dominated by the 8% uncertainty from experiment. This situation is an improvement over that before the CLEO measurement [8]. However, it is clear that a more stringent test of QCD would be possible with a smaller experimental error for the $J/\psi \to \eta_c\gamma$ branching fraction and this may become possible with BES III although it is a challenging mode [34, 35].

Our value for $V(0)$ corresponds to a width for $J/\psi \to \gamma\eta_c$ of 2.49(18)(7) keV using eq. (14). The first error is from our result and the second from the experimental error in $|\vec{q}|$. Note that in using eq. (14) we put in the experimental masses for the J/ψ and η_c. This is appropriate because these factors are kinematic ones and therefore should be taken to match the experiment. What we calculate in lattice QCD is $V(0)$. In fact, as discussed above, we have good agreement between our results and experiment for $M_{J/\psi} - M_{\eta_c}$ and so the kinematic factors would also be correct from lattice QCD. However, extra uncertainty would be introduced by using the lattice QCD results and that is not necessary or appropriate. Our result for the decay width corresponds to a branching fraction for $J/\psi \to \eta_c$ of 2.68(19)(11)%, where the first error is from our calculation and the second from experiment, including the experimental width of the J/ψ.

Figures 2, 3 and 7, which show our results as a function of lattice spacing, confirm that discretisation errors are small (although visible) for the HISQ formalism and that the approach to the continuum limit is well-controlled. This is discussed further in Appendix C where we compare the dependence on lattice spacing to that for twisted mass quarks [10].

V. CONCLUSIONS

We have given results for 3 key quantities associated with the J/ψ meson from lattice QCD, for the first time including the effect of all three u, d and s quarks in the sea. The quantities are the mass difference with its pseudoscalar partner, the η_c meson, the decay constant and the vector form factor at $q^2 = 0$ for $J/\psi \to \eta_c$ decay.

Our first key result is for the J/ψ decay constant. We obtain:

$$f_{J/\psi} = 405(6)\,\text{MeV}, \tag{29}$$

leading to $\Gamma(J/\psi \to e^+e^-) = 5.48(16)$ keV. This is to be compared to the experimental result of $\Gamma(J/\psi \to e^+e^-) = 5.55(14)$ keV [7]. We have therefore achieved a 4% test of lattice QCD from an electromagnetic decay rate (a 2% test from the decay constant), that does not suffer from CKM uncertainties. This is itself a stringent test of QCD and one for which lattice QCD is absolutely necessary; $f_{J/\psi}$ could not be calculated this accurately with any other method. At the same time we are able to verify that the time-moments of the J/ψ correlator agree as they should with results for the charm contribution to $\sigma(e^+e^- \to \text{hadrons})$ extracted from experiment. This is a test of QCD to better than 1.5%.

Our $f_{J/\psi}$ result is a critically important test for our calculations that determine the decay constants of the D_s [2, 36] and the D [36, 37] to a similar level of precision. In particular it tests the HISQ formalism for c quarks [11] even more stringently than in the D and D_s cases because the J/ψ contains two c quarks and is a smaller meson, more sensitive to discretisation effects on the lattice. Combined with our earlier work on using the HISQ formalism for light quarks in f_π and f_K [13, 36, 38], our result for $f_{J/\psi}$ provides compelling evidence that we have the systematic errors in f_{D_s} and f_D under control.

We can improve our result for $f_{J/\psi}$ further in future by using the vector form factor method of renormalisation rather than the current-current correlator method. This will only be useful if improved experimental results become available. This is expected from BESIII [35].

A further test of QCD/Lattice QCD comes from the J/ψ mass. We find:

$$M_{J/\psi} - M_{\eta_c} = 116.5 \pm 3.2\,\text{MeV} \tag{30}$$

giving $M_{J/\psi} = 3.0975(32)(11)\,\text{GeV}$ where the second error comes from the experimental average for M_{η_c} [7]. Experiment gives $M_{J/\psi} = 3.0969\,\text{GeV}$. This is another strong test of lattice QCD, and indeed QCD, against experiment to be compared to that of the determination

of M_{D_s} [2] and M_D [3]. The hyperfine splitting is a relatively small relativistic correction in the broader context of charmonium meson masses and the fact that we can do this well (with no free parameters) is because the HISQ formalism is such a highly improved relativistic formalism. This is underlined by a study of the meson dispersion relation (and associated 'speed of light') in Appendix C. In fact our error on $M_{J/\psi}$ is dominated by uncertainties from the effect of annihilation of the η_c meson to gluons, and it is important to pin these down more accurately.

Our third result for the J/ψ is that for its M1 radiative decay mode to the η_c. We find:

$$\Gamma(J/\psi \to \gamma\eta_c) = 2.49 \pm 0.19\,\mathrm{keV} \tag{31}$$

to be compared to the current experimental value of 1.84(30) keV [26]. The agreement is reasonably good, but the experimental error is large and the lattice QCD result would allow a much stronger test of QCD if this were reduced. This should be possible at BESIII [34]. Since the error in our lattice QCD result is dominated by the continuum extrapolation it will be improved in calculations on superfine and ultrafine lattices as we have done for the decay constant, and 2% errors should also be achievable here. Again, this is only possible in lattice QCD.

The $J/\psi \to \gamma\eta_c$ decay rate is another test of QCD, along with our leptonic decay constant, that is free of CKM uncertainties. It provides a validation of semileptonic decay rate calculations for D and D_s mesons [39–43], that also use HISQ quarks as well as a test of our techniques for nonperturbative current renormalisation that we are using for a range of semileptonic and radiative decays [41–43].

Acknowledgements We are grateful to the MILC collaboration for the use of their configurations and to C. DeTar, F. Sanfilippo, J. Simone and M. Steinhauser for useful discussions. Computing was done on the Darwin supercomputer at the University of Cambridge as part of the DiRAC facility jointly funded by STFC, BIS and the Universities of Cambridge and Glasgow and at the Argonne Leadership Computing Facility at Argonne National Laboratory, supported by the Office of Science of the U.S. Department of Energy under Contract DOE-AC02-06CH11357. We acknowledge the use of Chroma [44] for part of our analysis. Funding for this work came from MICINN (grants FPA2009-09638 and FPA2008-10732 and the Ramon y Cajal program), DGIID-DGA (grant 2007-E24/2), the DoE (DE-FG02-04ER41299), the EU (ITN-STRONGnet, PITN-GA-2009-238353), the NSF, the Royal Society, the Wolfson Foundation, the Scottish Universities Physics Alliance and STFC.

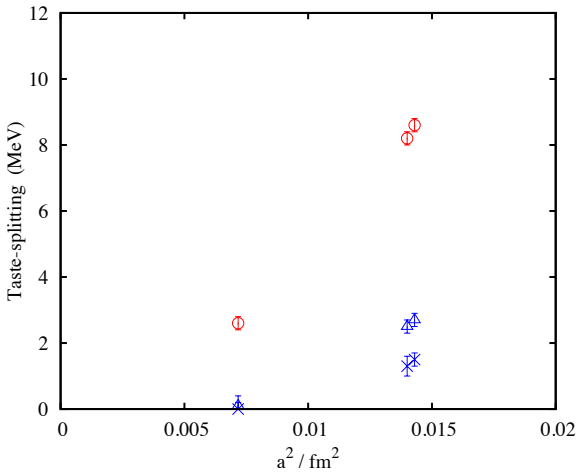

FIG. 11: Difference in mass in MeV for different meson 'tastes' for the η_c and J/ψ used here, plotted against the square of the lattice spacing. Red open circles show the mass difference between the local non-Goldstone and goldstone η_c mesons. For the vector we have the mass difference between the local J/ψ meson and the 1-link $\gamma_i \otimes \gamma_i\gamma_j$ vector (blue crosses) and the 1-link $\gamma_0\gamma_i \otimes \gamma_0\gamma_i\gamma_j$ vector (blue open triangles). The local J/ψ meson is the lighter in both cases. Results are for sets 1, 2 and 4 from Tables II and VI. Errors are statistical.

Appendix A: Taste effects in staggered mesons

Each staggered meson comes in 16 different tastes, most easily seen in terms of naive quark operators made with different point splittings:

$$J_n^{(s)} = \overline{\psi}(x)\gamma_n\psi(x+s). \tag{A1}$$

Here s is a 4-dimensional vector with 0 or 1 in each component. The different $J_n^{(s)}$ operators are orthogonal to each other. To work out the corresponding staggered quark correlators we need the staggering matrix, $\Omega(x)$. In our convention this is:

$$\Omega(x) = \prod_{\mu=1}^{4} (\gamma_\mu)^{x_\mu}, \tag{A2}$$

with $\gamma_4 \equiv \gamma_0$. Then the connection between naive quark propagators, which carry a spin index, and staggered quark propagators, which do not, is:

$$S_F(x,y) \equiv \langle\psi(x)\overline{\psi}(y)\rangle_\psi = g(x,y)\Omega(x)\Omega^\dagger(y). \tag{A3}$$

To work out the phases that appear in the correlator of a particular taste we then simply have to calculate spin traces over products of Ω and γ_n factors, see, for example, [11].

Here we use two different tastes for the η_c and three for the J/ψ and they all have slightly different masses. The mass differences between the different tastes of a

	$c_n^{(0)}$	$c_n^{(1)}$	$c_n^{(2)}$	$c_n^{(3)}$	$c_n^{(4)}$ ...
n=4	1.0	0.235	0.354	-0.187	0.0(5) ...
n=6	1.0	0.246	0.460	0.198	0.0(5) ...
n=8	1.0	0.253	0.563	0.511	0.0(5) ...

TABLE VII: The perturbative series [45–49] for the ratio r^P_{n+2}/r^V_n for different moments, n, in continuum QCD perturbation theory. $c_n^{(i)}$ is the coefficient of $\alpha^i_{\overline{MS}}(\mu = m)$; $c_n^{(0)}$ is 1.0 for all cases, by definition. $c_n^{(i)}$ for $i > 3$ were included in the determination of Z, allowing for a coefficient of 0.0 ± 0.5.

given meson, however, vanish as $\alpha_s^2 a^2$. For the η_c we use the Goldstone meson (in spin-taste notation this is the $\gamma_5 \otimes \gamma_5$ meson) and the local non-Goldstone meson (the $\gamma_0\gamma_5 \otimes \gamma_0\gamma_5$ meson), which are the first two mesons on the ladder of pseudoscalar tastes. We show the mass difference between them in Figure 11 for coarse and fine lattices. The mass difference amounts on the coarse lattices to a little less than 10 MeV (for a 3 GeV particle) and clearly falls with a^2 as expected. For the J/ψ we use the local vector ($\gamma_i \otimes \gamma_i$) and two 1-link operators which have a point-splitting in an orthogonal direction to the polarisation ($\gamma_i \otimes \gamma_i\gamma_j$ and $\gamma_0\gamma_i \otimes \gamma_i\gamma_j$). Note that these are not taste-singlet vectors. The mass difference between tastes for mesons of other J^{PC} is typically much smaller than for pseudoscalars and that is clear here. Figure 11 shows that the mass difference for the vectors is 1-2 MeV on the coarse lattices and not resolvable on the fine lattices.

In Section III C we showed results for $J/\psi \to \gamma\eta_c$ using different tastes of J/ψ and η_c at the two ends of the 3-point function. No difference was seen in the vector form factor at $q^2 = 0$ in the two cases, either on the coarse or fine lattices (within our statistical errors of 2%). This is another demonstration that taste effects are very small with HISQ quarks.

Appendix B: Determining nonperturbative Z factors for local vector currents

1. The current-current renormalization method

Time-moments of lattice QCD correlators for zero-momentum heavyonium mesons can be compared very accurately [50] to continuum QCD perturbation theory [45–49] developed for the analysis of the e^+e^- annihilation cross-section. This has been used with pseudoscalar meson correlators made with HISQ quarks to extract c and b masses and α_s to better than 1% [51]. These results used the goldstone pseudoscalar correlator, which is absolutely normalised because of the HISQ PCAC relation. Here we apply the same techniques to vector meson correlators but use it to determine the renormalisation factor, Z, required for the lattice vector current to match the continuum current.

The time moments of our lattice QCD correlators are defined as:

$$C_n^V = \sum_{\tilde{t}} \tilde{t}^n \overline{C}_{J/\psi}(\tilde{t}) \tag{B1}$$

and

$$C_n^P = \sum_{\tilde{t}} \tilde{t}^n (am_c)^2 \overline{C}_{\eta_c}(\tilde{t}) \tag{B2}$$

where $\tilde{t}$ is a symmetrised version of t around the centre of the lattice, i.e. going forward in time, $\tilde{t}$ runs from 0 to $L_t/2$ and then from $-L_t/2 + 1$ to -1. The extra factor of $(am_c)^2$ in the pseudoscalar case is to make a correlator moment which is finite as $a \to 0$. For both correlators we expect the small n moments to behave perturbatively, since they probe small times. Then our match to continuum perturbation theory is:

$$C_n^P = \frac{g_n^P(\alpha_{\overline{MS}}(\mu), \mu/m_c)}{(am_c(\mu))^{n-4}} + \mathcal{O}((am_c)^m). \tag{B3}$$

where g_n is the continuum QCD perturbation theory series in the $\overline{MS}$ scheme [45–49]. For the vector correlator a Z factor is needed to multiply the lattice current and so:

$$C_n^V = \frac{1}{Z^2} \frac{g_n^V(\alpha_{\overline{MS}}(\mu), \mu/m_c)}{(am_c(\mu))^{n-2}} + \mathcal{O}((am_c)^m). \tag{B4}$$

Z is then a function of the bare lattice strong coupling constant at each lattice spacing and so this match must be performed separately on each ensemble. By taking the ratio of pseudoscalar and vector moments we can cancel the factors of the quark mass. In fact we also divide each moment by its tree-level value (calculated with the gluon fields set to 1) to reduce discretisation errors, i.e. instead of C_n we use R_n where

$$R_n = \frac{C_n}{C_n^{(0)}} \tag{B5}$$

Set	$m_c a$	$Z(4) = Z_{cc}$	$Z(6)$	$Z(8)$
1	0.622	0.979(12)	0.945(14)	0.927(17)
2	0.63	0.979(12)	0.945(14)	0.926(17)
2	0.66	0.974(12)	0.941(14)	0.921(17)
4	0.413	0.983(12)	0.953(14)	0.953(17)
5	0.273	0.986(12)	0.970(14)	0.975(18)
6	0.193	0.990(12)	0.982(14)	0.986(18)

TABLE VIII: Renormalisation constants determined from the current-current correlator method on each configuration set used for the determination of $f_{J/\psi}$. The Z value we use is that from moment 4. The errors include an estimate of effects from a gluon condensate contribution, and unknown fourth order and higher terms in continuum perturbation theory. The errors are highly correlated between configuration sets (to better than 1% of the error). For set 2 we include both the tuned value of am_c (0.63) and the heavier, detuned, value (0.66). Very little difference is seen between them.

and also take the same ratio, calling it r_n, in the continuum perturbation theory. Finally Z is given by:

$$Z(n) = \sqrt{\frac{R^P_{n+2}/R^V_n}{r^P_{n+2}/r^V_n}}. \tag{B6}$$

Table VII gives the perturbative coefficients for the series in $\alpha_{\overline{MS}}(m)$ for r^P_{n+2}/r^V_n. This is known to 4-loops (α_s^3) and we include the possibility of unknown higher order terms (to 20th order) with prior values for the coefficients of 0 ± 0.5. We take $\mu = m$ but including the possibility of higher order corrections means that the results are almost completely insensitive to μ. We also allow for gluon condensate contributions taking $\alpha_s G^2/\pi = 0 \pm 0.012\,\mathrm{GeV}^4$. This increases the errors on the determination of the Z values as n increases.

Table VIII gives the results for Z on each ensemble and for moments 4, 6 and 8. The differences between the Z values on a given ensemble arise from discretisation errors. We take our final result for use in section III B from moment 4 (and so these numbers are reproduced in Table II) since, even though discretisation errors fall as the moment number increases, the errors from the gluon condensate rise more steeply. The error in $Z(4)$ is around 1%. It is dominated by the uncertainty in higher orders in perturbation theory and so strongly correlated from one lattice spacing to the next. We have checked that we obtain the same final result for f_ψ using Z(6) (but with an error of 1.6% rather than 1.4%).

2. The vector form factor method

Vector currents can be normalised completely nonperturbatively by requiring that the vector form factor at $q^2 = 0$ between two identical mesons be 1 since this would be true for a conserved vector current. We use this to normalise the staggered taste-singlet 1-link vector current between two mesons made of staggered quarks in [41]. Here, however, we want to normalise the taste-nonsinglet local staggered vector current, and we cannot do this using a 3-point function made entirely of staggered quarks. We have to include a non-staggered (and non-doubling) spectator quark in order to remove the requirement for overall taste-cancellation in the 3-point function [52]. The Fermilab Lattice/MILC collaboration use this method [53] with a clover spectator quark to normalise a light staggered vector current for the nonperturbative part of their mixed perturbative/nonperturbative approach to normalising the clover-staggered operators for heavy-light meson decay constants. Here we use an NRQCD spectator quark to normalise the local charm staggered vector current. In fact we can use any NRQCD-like action for the spectator since it does not need to correspond to a physical quark. However, for simplicity we do use the NRQCD action developed for our NRQCD-light spectrum calculations [3].

To combine an NRQCD (or other non-staggered) quark with a staggered quark we convert it to a naive quark [52],

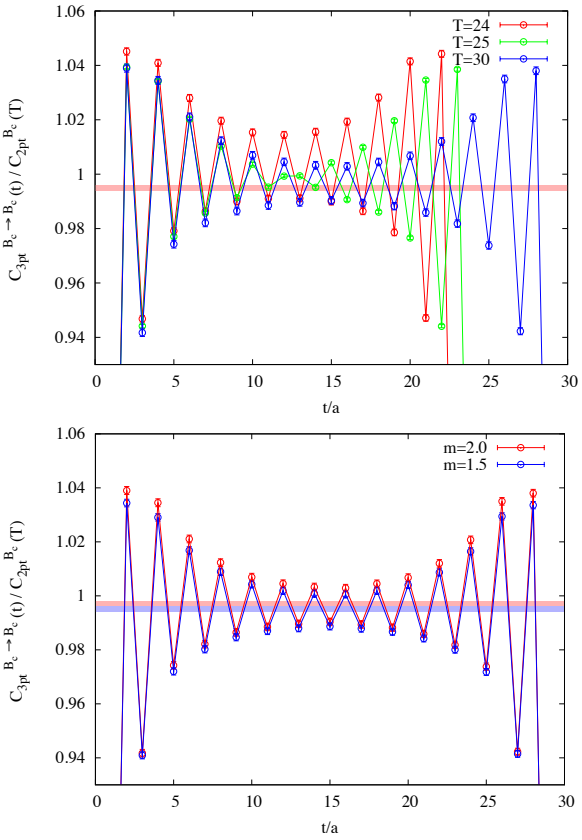

FIG. 12: The ratio of the 3-point function for the 'B_c' to 'B_c' vector form factor to the 'B_c' 2-point function against the source-current separation, t/a. The top plot shows results for $m_b a = 2.0$ on fine lattices, set 4, for various values of T. Lines join the points for clarity. The shaded red band gives our fit result for the ground state matrix element. The lower plot shows results, also on set 4, for two different values of $m_b a$. The shaded red and blue bands show the fit results for the ground state matrix elements.

re-instating the spin degree of freedom as in eq. (A3). A pseudoscalar meson correlator which, with two idential quarks, would simply be the sum over spins and colors of the squared modulus of the propagator, becomes in this case:

$$C_{Qq}(t) = \sum_{\vec{x},\vec{y}} \mathrm{Tr}\left\{G(x,y)\Omega(y)g^\dagger(x,y)\Omega^\dagger(x)\right\}. \tag{B7}$$

The trace is over spin and color but separates since the staggered propagator, $g(x,y)$, has no spin and Ω no color. Then:

$$C_{Qq}(t) = \sum_{\vec{x},\vec{y}} \mathrm{Tr}_c\left\{\mathrm{Tr}_s[\Omega^\dagger(x)G(x,y)\Omega(y)]g^\dagger(x,y)\right\}. \tag{B8}$$

This makes clear that we can transfer the Ω matrices to the non-staggered quark propagator, $G(x,y)$, and this allows us, as shown in [14], to combine staggered and non-staggered quarks from random wall sources. We simply

make the source of the non-staggered quark the product of $\Omega(y)$ (where y runs over a time slice at the source) with the random number at each y value in the random wall, convoluted with smearing functions if required. At the sink we multiply by $\Omega^\dagger$ before tracing over spins to combine with the spinless staggered quark propagator. Here we develop this method further for 3-point functions.

For the matrix element of the temporal charm-charm vector current between identical charmed pseudoscalar mesons, at rest, we have:

$$\langle P_c|V_t|P_c\rangle = 2m_{P_c} f_+(0) \tag{B9}$$

and we can demand that $f_+(0) = 1$, i.e. we can multiply the left-hand-side by Z to make this true. The temporal component of the vector current is the easiest to use for this purpose although the spatial component of the vector current is the one that we use for $J/\psi \to \eta_c$ decay. For a relativistic action such as HISQ the renormalisation of the spatial and temporal components will be the same up to discretisation errors.

For the 3-point function needed to evaluate the matrix element above we use an NRQCD heavy quark propagating from 0 to T and HISQ charm quarks from 0 to t and T to t (see Fig. 5). The local staggered temporal vector current ($\gamma_0 \otimes \gamma_0$ in spin-taste notation) is inserted at t and the restriction for staggered 3-point functions of an overall tasteless correlator is avoided by the spin content of the NRQCD propagator.

The 3-point function is given by:

$$C_{3pt}(0,t,T) = \sum_{s_T,s_t} (-1)^{x_T+y_T+z_T+t_T}(-1)^{t_t} \tag{B10}$$
$$\times \mathrm{Tr_c}\left\{g(t,T)\mathrm{Tr_s}[\gamma_0\Omega^\dagger(T)G(T,0)\Omega(0)]g^\dagger(t,0)\right\}$$

The g are HISQ c propagators and G is an NRQCD heavy quark propagator. The γ_0 factor comes from the local temporal vector current. The 3-point function is therefore calculated in a very similar way to the 2-point function. $\Omega(x)$ multiplied by the random wall at the source time slice, 0, is used as the source for the NRQCD propagator. At time T this is multiplied by $\Omega^\dagger$ and γ_0, source and sink spins are set equal and summed over. This is then the source for the HISQ propagator from T to t which is finally combined with the HISQ propagator generated from the random wall at time slice 0.

We calculate the 2-point and 3-point functions described above for several different NRQCD masses, $m_h a$, and c quark masses, $m_c a$, on the configuration sets 1, 2 and 4. We also use several different values of T so that our fit benefits from both T and t dependence to improve the extraction of the ground-state masses, amplitudes and matrix elements. The 3-point and 2-point correlators are fit simultaneously to the forms given in eqs (1) and (25). We use the same priors as in section III C. Note that for the 3-point fit we can now impose symmetry under interchange of the mesons at 0 and T since they are the same. This means that the amplitudes V^{nn} and V^{oo} are square symmetric matrices and $V^{no} = V^{on}$.

The key quantity that we extract from the fit is the ground state matrix element V^{nn}_{00}. This is proportional to the vector matrix element on the left-hand-side of eq. (B9). We can work out the constant of proportionality by matching our fit equations, eq (25) and (1) to the form expected by inserting a complete set of states in a continuum 3-point function. In this case factors of the mass of the meson[4] cancel and we find $V^{nn}_{00} = f_+(0)$. Then the renormalisation factor we need is given by:

$$Z = \frac{1}{V^{nn}_{00}}. \tag{B11}$$

The results for Z are taken from fits with 5 normal and 4 oscillating exponentials and given in Table IX. We obtain very precise results for Z, with errors of 0.1%, without even using the full statistics available for each ensemble. The values are much more precise, for example, than for the implementation given in [53] (although their values are for light quarks rather than charm).

Figure 12 shows the quality of our results through plots of the ratio of the 3-point to the 2-point function. Note that we fit the 3-point and 2-point functions simultaneously and *not* just the ratio. It is convenient to plot the ratio, however, because the ground state contribution to this is simply V^{nn}_{00}. Our fit allows us to include the effect of excited states, both normal states and oscillating states. The presence of oscillating states is evident in the plots. The upper plot of Figure 12 compares results at different T values. All are included in the simultaneous fit. The lower plot shows results at different values of $m_h a$ for a given $m_c a$.

The vector form factor method for determining Z is completely nonperturbative. It will therefore be subject to errors coming from lattice QCD in the form of discretisation errors. These mean, for example, that the Z factor at a particular value of the lattice spacing is not completely independent of the mass of the NRQCD spectator quark. From our results in Table IX we see that changing $m_h a$ from 2.8 to 1.5 on coarse set 2 (corresponding to change of almost a factor of two) causes a 2% change in Z. On fine set 4 the sensitivity is reduced to a change of 0.2%, not significant within our statistical errors, when $m_h a$ is changed from 2.0 to 1.5, a change in mass of 30%. Since the change in lattice spacing between the coarse and fine sets is a factor of 1.4, pairs of am_h values on coarse and fine lattices that correspond to approximately the same physical mass are (2.8, 2.0) and (2.0, 1.5). We will take our central result for Z_{ff} from the Z values corresponding to using (2.0, 1.5) and use (2.8, 2.0) to check systematic errors coming from Z. We see in section III C that we get the same answer from both sets of Z values.

[4] For a meson containing an NRQCD quark the energy obtained from the 2-point and 3-point fits is not its mass. However that is irrelevant here since it cancels.

Set	$N_{\rm cfg} \times N_t$	T	am_h	am_c	ϵ	aE_{P_c}	V_{00}^{nn}	$Z = Z_{ff}$
1	450×4	20,21	2.0	0.622	-0.221	0.9630(2)	1.0104(12)	0.9896(11)
2	408×4	20,21,24	2.8	0.63	-0.226	1.0239(2)	1.0220(10)	0.9784(9)
		20,21,24	2.0	0.63	-0.226	0.9719(2)	1.0106(8)	0.9894(8)
		20,21	1.5	0.63	-0.226	0.9311(3)	1.0026(14)	0.9974(14)
		20,21	2.0	0.66	-0.244	0.9994(3)	1.0138(18)	0.9863(17)
4	322×4	24,25,30	2.0	0.413	-0.107	0.6454(2)	0.9966(14)	1.0033(14)
		24,25,30	1.5	0.413	-0.107	0.5939(2)	0.9950(10)	1.0049(10)

TABLE IX: The Z factors (column 9) obtained from the vector form factor method on different configurations sets (column 1) and for different NRQCD quark masses, $m_h a$ (column 4), and c quark masses, $m_c a$ (column 5) with ϵ factor (column 6). The $m_c a$ values are those used in our calculation of $J/\psi \to \eta_c \gamma$ described in section III C; the $m_h a$ values are arbitrary since they correspond to the spectator quark. Z is given by the inverse of the fit parameter V_{00}^{nn} given in column 8. Column 2 gives the number of configurations used in the calculation and the number of time sources for the origin, 0. The T values used are given in column 3. Column 7 gives the energy of the NRQCD-c meson obtained from the fit. This is not equal to the mass because there is an energy offset in NRQCD.

Set	$m_c a$	aM_{η_c}	$\lvert a\vec{p}\rvert$	aE_{η_c}	c^2
2	0.63	1.80851(4)	0.52880	1.88286(12)	0.9814(15)
			0.35000	1.84123(5)	0.9748(5)
			0.20000	1.81923(4)	0.9715(6)
4	0.413	1.28042(4)	0.37486	1.33352(6)	0.9878(8)
			0.20000	1.29575(4)	0.9873(7)

TABLE X: Rest masses (aM_{η_c}) and energies (aE_{η_c}) at non-zero momentum $|a\vec{p}|$ for the Goldstone η_c meson on sets 2 (coarse) and 4 (fine). The rest masses differ slightly from those in Table II because they come from independent fits; on set 4 we have higher statistics here. The zero and non-zero momentum correlator are fitted simultaneously and the speed of light, c^2, extracted using eq. (C1).

Table IX also shows results for the deliberately mistuned c quark mass of 0.66 on set 2 with which we test the c quark mass dependence of our $J/\psi \to \eta_c$ form factor. A barely significant change in Z is seen between this value and that for the tuned mass of 0.63. We also see no significant difference in Z as we change the sea light quark masses between set 1 and set 2.

Discretisation errors also mean that our results for Z_{ff} here do not have to agree exactly with our earlier results for Z_{cc}. Z_{cc} has a much larger error coming from unknown higher order terms in continuum perturbation theory. As a result of this, Z_{ff} and Z_{cc} do agree at the level of 1σ. They also agree within errors with the lattice QCD perturbation theory for this renormalisation, which has a small negative contribution at $\mathcal{O}(\alpha_s)$ [54].

The Z values calculated here form part of a programme to normalise nonperturbatively a range of staggered currents for a variety of weak semileptonic and electromagnetic radiative decay rates [42].

Appendix C: Discretisation errors

Finally we discuss discretisation errors. For relativistic formalisms the scale of discretisation errors can be set by the quark mass when this is larger than Λ_{QCD} and

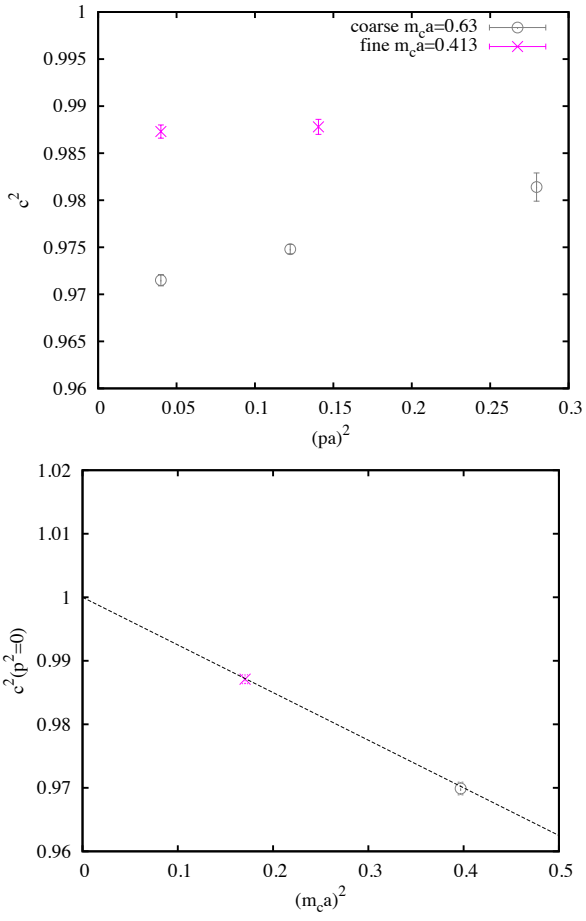

FIG. 13: The 'speed-of-light', c^2, calculated from zero and finite momentum η_c correlators using HISQ c quarks. The top figure shows c^2 as a function of the square of the spatial momentum for coarse lattices, set 2, where $m_c a = 0.63$ (grey open circles) and for fine lattices, set 4, where $m_c a = 0.413$ (pink crosses). The lower figure shows the resulting values of c^2 as $\vec{p}^2 a^2 \to 0$ as a function of $(m_c a)^2$. The dashed straight line is drawn to guide the eye.

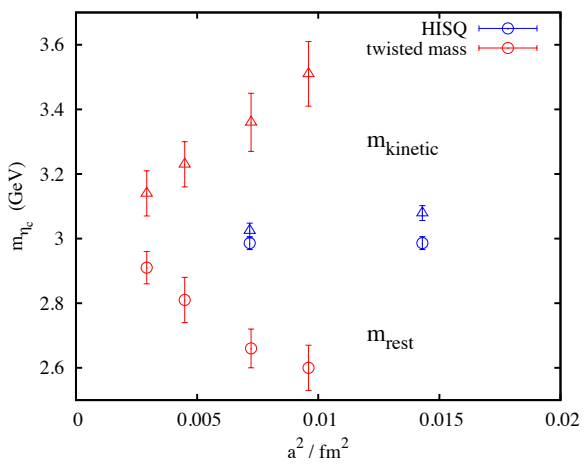

FIG. 14: The rest (static) and kinetic masses for the η_c meson compared between the HISQ formalism (this paper) and the twisted mass formalism (Figure 3 from [10]), and plotted against the square of the lattice spacing. The rest mass is given by open circles and the kinetic mass by open triangles, red for twisted mass and blue for HISQ. Errors include the full lattice spacing error on each point.

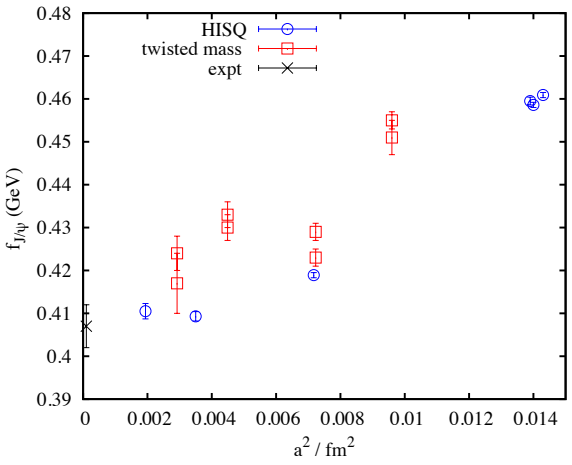

FIG. 16: $f_{J/\psi}$ in GeV is plotted against a^2 in fm^2 for the HISQ formalism (this paper, blue open circles) and for twisted mass ([10], red open squares). For the twisted mass case the heaviest and lightest sea quark masses are plotted at each value of the lattice spacing. Only statistical errors are shown for the twisted mass results. For the HISQ results we show the raw data from Table II with statistical and uncorrelated lattice spacing errors. There is an additional error of 1.3% from correlated lattice spacing and Z factor uncertainties. The black cross is the experimental result from the average leptonic width [7], offset slightly from the origin for clarity.

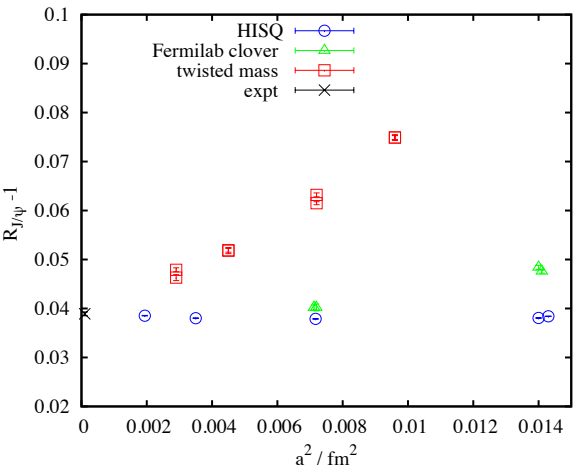

FIG. 15: $R_{J/\psi} - 1$ plotted against a^2 in fm^2 for three different quark formalisms for the c quark: HISQ (this paper, blue open circles), twisted mass ([10], red open squares) and Fermilab clover ([29], green open triangles, showing results on the two finest lattices only). $R_{J/\psi}$ is $M_{J/\psi}/M_{\eta_c}$ so $R_{J/\psi} - 1 = \Delta M_{hyp}/M_{\eta_c}$. For the twisted mass and Fermilab clover results the heaviest and lightest sea quark masses are plotted at each value of the lattice spacing. Only statistical errors are shown. Additional errors from (twice) the lattice spacing error amount to 2% for HISQ and Fermilab clover and 4-7% for twisted mass. The black cross is the experimental average [7], offset slightly from the origin for clarity.

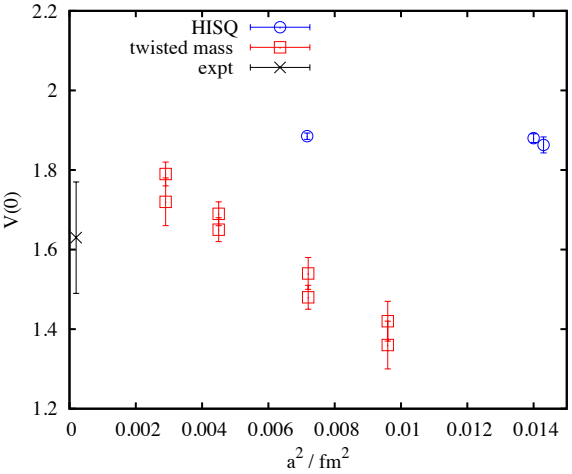

FIG. 17: The vector form factor for $J/\psi \to \eta_c$ decay at $q^2 = 0$, $V(0)$, is plotted against a^2 in fm^2 for the HISQ formalism (this paper, jpsigamma0 method, blue open circles) and for twisted mass ([10], red open squares). For the twisted mass case the heaviest and lightest sea quark masses are plotted at each value of the lattice spacing. Errors include statistical errors and uncertainties in the Z factors. The black cross is the experimental result from the rate for $J/\psi \to \eta_c\gamma$ decay [26], offset slightly from the origin for clarity.

so they must be monitored closely when working with c quarks.

One simple way to do this is through study of the energy of mesons at non-zero spatial momentum. Because the HISQ formalism is a relativistic formalism we determine meson masses as the result of fitting zero-momentum meson correlators as described in section II. For heavy quarks discretisation errors mean that this mass, known as the 'rest' or 'static' mass, can differ from the mass that controls the momentum-dependence of the energy at non-zero spatial momentum. This latter mass is known as the 'kinetic mass'. An equivalent statement is that the square of the speed-of-light, c^2, differs from 1, where [11]

$$c^2(\vec{p}) = \frac{E^2(\vec{p}) - m^2}{\vec{p}^2}. \tag{C1}$$

For η_c mesons we are able to determine c^2 very accurately with HISQ quarks when we have $\mathcal{O}(10,000)$ correlators as here. We fit zero and non-zero momentum simultaneously to the form given in eq. (1) (although the zero momentum correlators have no oscillating component). From the fit we obtain the ground state mass, M_0, in the zero momentum case and the ground state energy, E_0, in the non-zero momentum case. The simultaneous fit allows us to take correlations into account to improve the error in c^2. Results are given in Table X. c^2 is within 3% of 1 but we can distinguish it from 1 and we can see that it depends on the spatial momentum. This is shown in the top plot of Figure 13 for the coarse lattices, set 2, and the fine lattices, set 4. All tree-level a^2 errors are removed in HISQ but c^2 can depend linearly on $a^2\vec{p}^2$ through $\mathcal{O}(\alpha_s)$ corrections. We see that the slope of c^2 with $a^2\vec{p}^2$ is much smaller on the fine lattices than the coarse, as $m_c a$ is reduced. This plot can be compared with earlier results in Figure 9 of [55], although note that those results show a jump as the lattice momentum changes from (1,1,1) to (2,0,0). This results from a rotationally-noninvariant discretisation error not evident in our results because of the use of the phased boundary condition of eq. (16) to fix the momentum direction and simply change its magnitude.

From the top plot of Figure 13 we can determine the value of c^2 at $a^2\vec{p}^2 = 0$. The results from the coarse and fine lattices are then shown in the lower plot to lie on a straight line as a function of $(m_c a)^2$. The small slope is compatible with the $(m_c a)^2$ dependence also being an $\mathcal{O}(\alpha_s)$ effect. The straight line clearly goes through 1 as $m_c a \to 0$ as it must.

Another way to look at these discretisation errors is to compare the rest and kinetic masses for the η_c. The kinetic mass is given by [56]:

$$M_{kin} = \frac{|\vec{p}|^2 - (\Delta E)^2}{2\Delta E} \tag{C2}$$

where $\Delta E = E(\vec{p}) - M_{rest}$. We also have $c^2 = M_{rest}/M_{kin}$ [11]. In the absence of errors, for a relativistic formalism, we should have $M_{rest} = M_{kin}$ (i.e. $c^2 = 1$). In Figure 14 we compare the rest and kinetic masses for HISQ η_c mesons using $M_{kin} = M_{rest}/(c^2(\vec{p}^2 = 0))$ determined from Figure 13. The rest and kinetic masses differ by 3% on the coarse lattices and 1.3% on the fine lattices.

Figure 14 also compares results from the twisted mass formalism, from [10]. For that formalism there is a significantly larger difference between rest and kinetic masses for the η_c meson, amounting to 35% on the coarsest lattice spacing. The twisted mass formalism has tree-level a^2 errors, so a larger effect would be expected. The rest and kinetic masses agree in the continuum limit, as they must.

Figure 15 compares the hyperfine splitting in charmonium in units of the η_c mass as a function of the square of the lattice spacing for the HISQ and twisted mass formalisms. The quantity plotted is $R_{J/\psi} - 1$ where $R_{J/\psi}$ is defined in [10] as $M_{J/\psi}/M_{\eta_c}$ and results are given on each of their ensembles. The HISQ results are taken from Table II. We also show results from the Fermilab clover method [29] on their two finest sets of ensembles which correspond to the coarse and fine lattices used here.

All the results tend to the same continuum value which agrees with experiment. Much larger discretisation effects are visible for the twisted mass formalism than for HISQ. These are compatible with the tree level a^2 errors expected in that formalism, and with a mass scale of approximately 2 GeV (i.e. m_c). These tree level errors are removed in the HISQ formalism, but $\alpha_s a^2$ errors remain. These seem to be small for this quantity. The Fermilab clover discretisation errors, although in principle $\alpha_s a$, are also relatively small over this range of a.

Discretisation effects in the hyperfine splitting can also enter through tuning of the c quark mass, because the hyperfine splitting is very sensitive to this. As discussed earlier in this section, there can be significant differences between rest and kinetic masses for mesons made of heavy quarks, and either can be used to tune the quark mass. Both relativistic formalisms, HISQ and twisted mass, use the rest mass. The Fermilab formalism uses the kinetic mass.

For $f_{J/\psi}$ the difference in discretisation effects between the HISQ and twisted mass formalisms is not as large. This is shown in Figure 16. Again, answers in agreement are obtained in the continuum limit. For the moments of the vector correlator our results for G_4^V (Fig 4), which show very little dependence on the lattice spacing, can be compared to those for the twisted mass formalism in [57], where somewhat larger discretisation effects are visible.

Finally in Figure 17 we compare results for the vector form factor for $J/\psi \to \eta_c$ decay, $V(0)$. Large discretisation effects are evident in the twisted mass results. Once again discretisation effects in the HISQ results are small. Agreement in the continuum limit is again clear, however.

The HISQ results shown here give a further and more testing demonstration than that of [11, 36] of how small the discretisation errors for the HISQ action are, even for a quark as heavy as charm.

[1] C. Davies et al. (HPQCD, UKQCD, MILC and Fermilab Lattice Collaborations), Phys.Rev.Lett. **92**, 022001 (2004), hep-lat/0304004.

[2] C. Davies, C. McNeile, E. Follana, G. Lepage, H. Na, et al. (HPQCD Collaboration), Phys.Rev. **D82**, 114504 (2010), 1008.4018.

[3] R. Dowdall, C. Davies, T. Hammant, and R. Horgan (HPQCD Collaboration) (2012), 1207.5149.

[4] C. Davies, PoS **LATTICE2011**, 019 (2011), 1203.3862.

[5] J. Laiho, E. Lunghi, and R. Van de Water, PoS **LATTICE2011**, 018 (2011), 1204.0791.

[6] A. Bazavov et al. (MILC Collaboration), PoS **LATTICE2010**, 074 (2010), 1012.0868.

[7] J. Beringer et al. (Particle Data Group), Phys. Rev. **D86**, 010001 (2012).

[8] J. J. Dudek, R. G. Edwards, and D. G. Richards, Phys.Rev. **D73**, 074507 (2006), hep-ph/0601137.

[9] Y. Chen, D.-C. Du, B.-Z. Guo, N. Li, C. Liu, et al., Phys.Rev. **D84**, 034503 (2011), 1104.2655.

[10] D. Becirevic and F. Sanfilippo (2012), 1206.1445.

[11] E. Follana et al. (HPQCD Collaboration), Phys.Rev. **D75**, 054502 (2007), hep-lat/0610092.

[12] A. Bazavov, D. Toussaint, C. Bernard, J. Laiho, C. DeTar, et al., Rev.Mod.Phys. **82**, 1349 (2010), 0903.3598.

[13] C. Davies, E. Follana, I. Kendall, G. P. Lepage, and C. McNeile (HPQCD Collaboration), Phys.Rev. **D81**, 034506 (2010), 0910.1229.

[14] E. B. Gregory, C. T. Davies, I. D. Kendall, J. Koponen, K. Wong, et al. (HPQCD Collaboration), Phys.Rev. **D83**, 014506 (2011), 1010.3848.

[15] G. P. Lepage et al., Nucl. Phys. Proc. Suppl. **106**, 12 (2002), hep-lat/0110175.

[16] C. Davies et al. (UKQCD Collaboration), Phys.Rev. **D58**, 054505 (1998), hep-lat/9802024.

[17] L. Levkova and C. DeTar, Phys.Rev. **D83**, 074504 (2011), 1012.1837.

[18] A. Vinokurova et al. (Belle collaboration), Phys.Lett. **B706**, 139 (2011), 1105.0978.

[19] M. Ablikim et al. (BESIII Collaboration), Phys.Rev.Lett. **108**, 222002 (2012), 1111.0398.

[20] J. Erler, Phys.Rev. **D59**, 054008 (1999), hep-ph/9803453.

[21] G. Adams et al. (CLEO Collaboration), Phys.Rev.Lett. **101**, 101801 (2008), 0806.0671.

[22] J. H. Kuhn, M. Steinhauser, and C. Sturm, Nucl.Phys. **B778**, 192 (2007), hep-ph/0702103.

[23] B. Dehnadi, A. H. Hoang, V. Mateu, and S. M. Zebarjad (2011), 1102.2264.

[24] E. Eichten, S. Godfrey, H. Mahlke, and J. L. Rosner, Rev.Mod.Phys. **80**, 1161 (2008), hep-ph/0701208.

[25] N. Brambilla, S. Eidelman, B. Heltsley, R. Vogt, G. Bodwin, et al., Eur.Phys.J. **C71**, 1534 (2011), 1010.5827.

[26] R. Mitchell et al. (CLEO Collaboration), Phys.Rev.Lett. **102**, 011801 (2009), 0805.0252.

[27] G. de Divitiis, R. Petronzio, and N. Tantalo, Phys.Lett. **B595**, 408 (2004), hep-lat/0405002.

[28] D. Guadagnoli, F. Mescia, and S. Simula, Phys.Rev. **D73**, 114504 (2006), hep-lat/0512020.

[29] T. Burch, C. DeTar, M. Di Pierro, A. El-Khadra, E. Freeland, et al., Phys.Rev. **D81**, 034508 (2010), 0912.2701.

[30] L. Liu, G. Moir, M. Peardon, S. M. Ryan, C. E. Thomas, et al. (2012), 1204.5425.

[31] G. S. Bali, S. Collins, and C. Ehmann, Phys.Rev. **D84**, 094506 (2011), 1110.2381.

[32] Y. Namekawa et al. (PACS-CS Collaboration), Phys.Rev. **D84**, 074505 (2011), 1104.4600.

[33] D. Mohler and R. Woloshyn, Phys.Rev. **D84**, 054505 (2011), 1103.5506.

[34] D. Asner, T. Barnes, J. Bian, I. Bigi, N. Brambilla, et al., Int.J.Mod.Phys. **A24**, S1 (2009), 0809.1869.

[35] C. Yuan, private communication (2012).

[36] E. Follana, C. Davies, G. Lepage, and J. Shigemitsu (HPQCD Collaboration), Phys.Rev.Lett. **100**, 062002 (2008), 0706.1726.

[37] H. Na, C. T. Davies, E. Follana, G. P. Lepage, and J. Shigemitsu (HPQCD Collaboration) (2012), 1206.4936.

[38] R. Dowdall et al. (HPQCD Collaboration), Phys.Rev. **D85**, 054509 (2012), 1110.6887.

[39] H. Na, C. T. Davies, E. Follana, G. P. Lepage, and J. Shigemitsu (HPQCD Collaboration), Phys.Rev. **D82**, 114506 (2010), 1008.4562.

[40] H. Na, C. T. Davies, E. Follana, J. Koponen, G. P. Lepage, et al. (HPQCD Collaboration), Phys.Rev. **D84**, 114505 (2011), 1109.1501.

[41] J. Koponen et al. (HPQCD Collaboration), PoS **LATTICE2011**, 286 (2011), 1111.0225.

[42] G. Donald, C. Davies, and J. Koponen (HPQCD Collaboration), PoS **LATTICE2011**, 278 (2011), 1111.0254.

[43] G. Donald, J. Koponen, et al. (HPQCD Collaboration), in preparation (2012).

[44] R. G. Edwards and B. Joo (SciDAC, LHPC and UKQCD Collaborations), Nucl.Phys.Proc.Suppl. **140**, 832 (2005), hep-lat/0409003.

[45] K. Chetyrkin, J. H. Kuhn, and C. Sturm, Eur.Phys.J. **C48**, 107 (2006), hep-ph/0604234.

[46] R. Boughezal, M. Czakon, and T. Schutzmeier, Phys.Rev. **D74**, 074006 (2006), hep-ph/0605023.

[47] A. Maier, P. Maierhofer, and P. Marqaurd, Phys.Lett. **B669**, 88 (2008), 0806.3405.

[48] A. Maier, P. Maierhofer, P. Marquard, and A. Smirnov, Nucl.Phys. **B824**, 1 (2010), 0907.2117.

[49] Y. Kiyo, A. Maier, P. Maierhofer, and P. Marquard, Nucl.Phys. **B823**, 269 (2009), 0907.2120.

[50] I. Allison et al., Phys.Rev. **D78**, 054513 (2008), 0805.2999.

[51] C. McNeile, C. Davies, E. Follana, K. Hornbostel, and G. Lepage (HPQCD Collaboration), Phys.Rev. **D82**, 034512 (2010), 1004.4285.

[52] M. Wingate, J. Shigemitsu, C. T. Davies, G. P. Lepage, and H. D. Trottier (HPQCD Collaboration), Phys.Rev. **D67**, 054505 (2003), hep-lat/0211014.

[53] A. Bazavov et al. (Fermilab Lattice and MILC Collaborations), Phys.Rev. **D85**, 114506 (2012), 1112.3051.

[54] H. Trottier, private communication (2008).

[55] A. Bazavov et al. (MILC collaboration), Phys.Rev. **D82**, 074501 (2010), 1004.0342.

[56] A. Gray, I. Allison, C. Davies, E. Dalgic, G. Lepage, et al. (HPQCD Collaboration), Phys.Rev. **D72**, 094507 (2005), hep-lat/0507013.

[57] K. Jansen, M. Petschlies, and C. Urbach, PoS **LATTICE2011**, 234 (2011), 1111.5252.